# nature communications



**Article** 

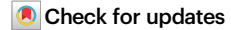
https://doi.org/10.1038/s41467-024-52970-7

# A subpellicular microtubule dynein transport machinery regulates ookinete morphogenesis for mosquito transmission of *Plasmodium yoelii*

Received: 28 June 2024

Accepted: 25 September 2024

Published online: 04 October 2024



Bing Liu<sup>1,4</sup>, Cong Liu<sup>2,4</sup>, Zhenkui Li<sup>3,4</sup>, Wenjia Liu ®¹, Huiting Cui ®¹⊠ & Jing Yuan ®¹⊠

The cortical cytoskeleton of subpellicular microtubules (SPMTs) supports the *Plasmodium* ookinete morphogenesis during mosquito transmission of malaria. SPMTs are hypothesized to function as the cytoskeletal tracks in motor-driven cargo transport for apical organelle and structure assembly in ookinetes. However, the SPMT-based transport motor has not been identified in the *Plasmodium*. The cytoplasmic dynein is the motor moving towards the minus end of microtubules (MTs) and likely be responsible for cargo transport to the apical part in ookinetes. Here we screen 7 putative dynein heavy chain (DHC) proteins in the *P. voelii* and identify DHC3 showing peripheral localization in ookinetes. DHC3 is localized at SPMTs throughout ookinete morphogenesis. We also identify five other dynein subunits localizing at SPMTs. DHC3 disruption impairs ookinete development, shape, and gliding, leading to failure in mosquito infection of *Plasmodium*. The DHC3-deficient ookinetes display defective formation or localization of apical organelles and structures. Rab11A and Rab11B interact with DHC3 at SPMTs in a DHC3-dependent manner, likely functioning as the receptors for the cargoes driven by SPMT-dynein. Disturbing Rab11A or Rab11B phenocopies DHC3 deficiency in ookinete morphogenesis. Our study reveals an SPMT-based dynein motor driving the transport of Rab11A- and Rab11B-labeled cargoes in the ookinete morphogenesis of Plasmodium.

Malaria remains a global infectious disease caused by unicellular apicomplexan protozoa of the genus *Plasmodium*, resulting in 627,000 deaths globally in 2022<sup>1</sup>. Malaria transmission relies on successful infection and development of *Plasmodium* in the female *Anopheles* mosquito vector. Once entering the mosquito midgut

after a blood meal, gametocytes are quickly activated to gametes that fertilize to form the zygotes. Within 12–24 h, a spherical zygote undergoes remarkable morphogenesis to differentiate into a crescent ookinete<sup>2–4</sup>. Only mature ookinetes are capable of gliding and traversing the mosquito midgut wall to colonize at the basal lumen

<sup>1</sup>State Key Laboratory of Cellular Stress Biology, School of Life Sciences, Faculty of Medicine and Life Sciences, Xiamen University, Xiamen, China.

<sup>2</sup>Department of Health Inspection and Quarantine, School of Public Health, Hengyang Medical School, University of South China, Hengyang, China.

<sup>3</sup>Institute of Pathogenic Biology and Key Laboratory of Special Pathogen Prevention and Control of Hunan Province, School of Basic Medical Sciences, Hengyang Medical School, University of South China, Hengyang, China.

<sup>4</sup>These authors contributed equally: Bing Liu, Cong Liu, Zhenkui Li.

© e-mail: cuihuiting@xmu.edu.cn; yuaniing@xmu.edu.cn

where thousands of sporozoites develop within an oocyst for parasite transmission<sup>5</sup>.

The invasive "zoite" stages of apicomplexan organisms, including the *Plasmodium* ookinete, sporozoite, and merozoite, as well as the Toxoplasma gondii tachyzoite, are morphologically polarized and possess a unique cortical pellicle underneath the parasite plasma membrane<sup>6,7</sup>. From outside to inside, the pellicle consists of a doublemembrane organelle inner membrane complex (IMC) and a cytoskeleton layer of apically radiating subpellicular microtubules (SPMTs), both of which associate with each other and span along the periphery of the zoite parasites<sup>6,7</sup>. Variable numbers of SPMTs are assembled in different zoite stages of *Plasmodium*, around 60 SPMTs in ookinetes<sup>8</sup>, 11-16 SPMTs in sporozoites<sup>9-11</sup>, and 1-9 SPMTs in merozoites<sup>8,11,12</sup>. Applying ultrastructure expansion microscopy (U-ExM), Bertiaux and Qian observed a super-high resolution cytoskeleton of SPMTs in the ookinetes of P. berghei and P. yoelii8,13. Besides SPMTs, the invasive zoites of apicomplexan parasites possess a highly specialized structure called the apical polar ring (APR) at the cell apical cortex. APR is recognized as an electron-lucent region beneath the apical IMC<sup>11,14,15</sup>, and resembles a cap-like structure in the transmission electron micrograph of the ookinetes<sup>11,16</sup>. Since the minus-ends of all SPMTs emanate from APR, it is believed that APR functions as a microtubuleorganizing center (MTOC) for nucleating SPMTs at the Plasmodium zoites<sup>7,17,18</sup>. In *Plasmodium*, the SPMT cytoskeleton functions as a scaffold supporting parasite morphogenesis4, maintaining the polarized cell shapes9 and providing parasite rigidity during gliding and invasion<sup>19</sup>. Another possible role of SPMTs is for docking the apical secretory organelles<sup>19</sup>, whose protein secretion mediates through a putative apical gateway for parasite gliding and invasion. So far, the roles of SPMTs in the invasive zoites of apicomplexan parasites remain incompletely understood.

The Plasmodium zygote to ookinete morphogenesis is orchestrated by two cellular processes, one is the ookinete growth via apical protrusion-elongation-maturation, and the other is the zygote contraction. In the process of ookinete growth, the parasite undergoes massive expansion of the plasma and cortex membrane. In addition, the ookinete acquires a complete set of apical organelles and structures via de novo assembly. IMC is assembled at the apical site of the initial protrusion and extends along the expanding plasma membrane to the basal end. After biogenesis, APR nucleates the assembly of apical SPMTs underling the IMC. Meanwhile, the apical tubulin ring (ATR), another compacted structure of MTs, emerges at the apex of ookinetes. Up to ookinete maturation, a number of the secretory organelle micronemes are distributed apically for protein secretion via exocytosis through the apex gateway. While the IMC, SPMT, APR, ATR, and microneme are essential for either development, gliding, or midgut invasion of ookinetes, the mechanisms for de novo assembly of these organelles and structures at the apical distal area are largely unknown.

Each apical organelle and structure contains a distinct set of component proteins<sup>20</sup>, all of which must find the way after synthesis from ER-Golgi near the nucleus to be delivered to the apical end of the ookinetes. In eukaryotes, intracellular cargoes like organelles, vesicles, proteins, and other molecules are trafficked by molecular motors that track along MTs or actin filaments throughout the cytoplasm<sup>21</sup>. MTs are polarized polymer structures with a minus end and a plus end<sup>22,23</sup>. The MT-based molecular motors, dynein (minus-end-directed) and kinesin (primarily plus-end-directed) are responsible for many types of intracellular transport<sup>24,25</sup>. As the retrograde motor, the cytoplasmic dynein is the principal motor in the cytoplasm<sup>26</sup>, while the axonemal dynein specifically drives the beating of flagellar and cilia<sup>27</sup>. Therefore, we hypothesize that besides playing a cytoskeleton role, the apically radiating SPMTs may function as the tracks for the apical transport of cargoes containing the contents required for the assembly of apical organelles and structures in the ookinetes<sup>7</sup>. In this scenario, the cytoplasmic dynein could be the primary motor moving towards the minus end of SPMTs for cargo transport to the apical distal area of ookinetes. However, the SPMT-based dynein transport machinery has not been identified in *Plasmodium*. Cytoplasmic dynein is a large multi-subunit protein complex, and the core is a homodimer of two heavy chain subunits (DHCs) interacting with intermediate, light intermediate, and light chain subunits<sup>25</sup>.

Here we screen the putative DHC genes in the genome of rodent malaria parasite *P. yoelii*. We identify the core subunit DHC3 and other subunits of dynein showing co-localizing with SPMTs in the ookinete. In-depth phenotypical and functional analyses demonstrate that SPMT-based dynein plays an essential role in ookinete morphogenesis, shape, and gliding motility. In addition, we find that two small GTPase proteins Rab11A and Rab11B may function as the receptors for the vesicle cargoes driven by SPMT-dynein. This study confirms the existence of the SPMT-based cytoplasmic dynein motor in the ookinetes and reveals its importance in intracellular cargo transport in ookinete morphogenesis.

#### Results

# Protein screening identifies a subpellicular dynein heavy chain DHC3 in ookinetes of *P. yoelii*

Each dynein contains at least one dynein heavy chain (DHC) and other subunits including the intermediate chain (IC), light intermediate chain (LIC), and light chain (LC)<sup>28</sup>. There are 7 genes encoding putative DHC proteins from the PlasmoDB database of the Plasmodium parasites. In the rodent malaria parasite P. yoelii, they are PY17X\_0418900 (dhc1),PY17X\_0618400 (dhc2),PY17X\_0215400 PY17X 0508400 (dhc4), PY17X 0927400 (dhc5), PY17X 0603800 (dhc6), and PY17X\_1333900 (dhc7) (Fig. 1A). These proteins range in size from 5063 to 6473 amino acids and are conserved among Plasmodium species. So far, the cytoplasmic and axonemal types of these DHCs remained undefined. To search for the potential SPMT-based cytoplasmic dynein in the ookinetes (Fig. 1A), we analyzed the expression and localization of these proteins in *P. yoelii*. Each gene was tagged with a sextuple HA epitope (6HA) at the C-terminus in the 17XNL strain using CRISPR-Cas9<sup>29,30</sup>. These 6HA-tagged parasite lines showed normal asexual blood stage proliferation and gametocyte differentiation in mice, suggesting that the addition of 6HA did not affect parasite viability. We next investigated the expression of these DHCs during the life cycle of the parasite. Immunofluorescence assay (IFA) showed that all these 7 DHCs displayed no detectable expression in the asexual blood stages (Fig. S1A). Only DHC3 was expressed in female gametocytes, ookinetes, and sporozoites (Fig. 1B and Fig. S1A-D). Other 6 DHCs (DHC1, DHC2, DHC4, DHC5, DHC6, and DHC7) were specifically expressed in male gametocytes (Fig. S1A-C). Notably, DHC3 was evenly distributed along the periphery of ookinetes (Fig. 1B), suggesting the existence of SPMT-based dynein in the ookinetes. Two parasite lines dhc3::3V5 and 4Myc::dhc3 were generated with endogenous DHC3 tagged with 3V5 at the C-terminus and with 4Myc at the N-terminus, respectively. Both DHC3::3V5 and 4Myc::DHC3 proteins displayed similar localization at the ookinetes (Fig. 1C, D). To visualize DHC3 localization in living ookinetes, we generated a parasite line, dhc3::mScarlet, with DHC3 C-terminally tagged with a red fluorescence protein mScarlet. The mScarlet-tagged DHC3 was also distributed along the periphery of ookinetes (Fig. 1E). These results suggested the existence of the SPMT-based cytoplasmic dynein in the ookinetes and DHC3 is likely a subunit of the dynein complex.

We analyzed the localization of DHC3 relative to proteins known to be expressed within specific localizations in ookinetes. We engineered parasite clones with additional proteins tagged with quadruple Myc epitope (4Myc) or triple V5 epitope (3V5) from the *dhc3::6HA* parasite. These proteins included P28 (plasma membrane), GAP45 (IMC) [14], MyosinB and SAS6L (apical tubulin ring, ATR)<sup>31,32</sup>, APR2 (apical polar ring, APR)<sup>13</sup>, GCβ (ookinete extrados site, OES)<sup>33</sup>, and

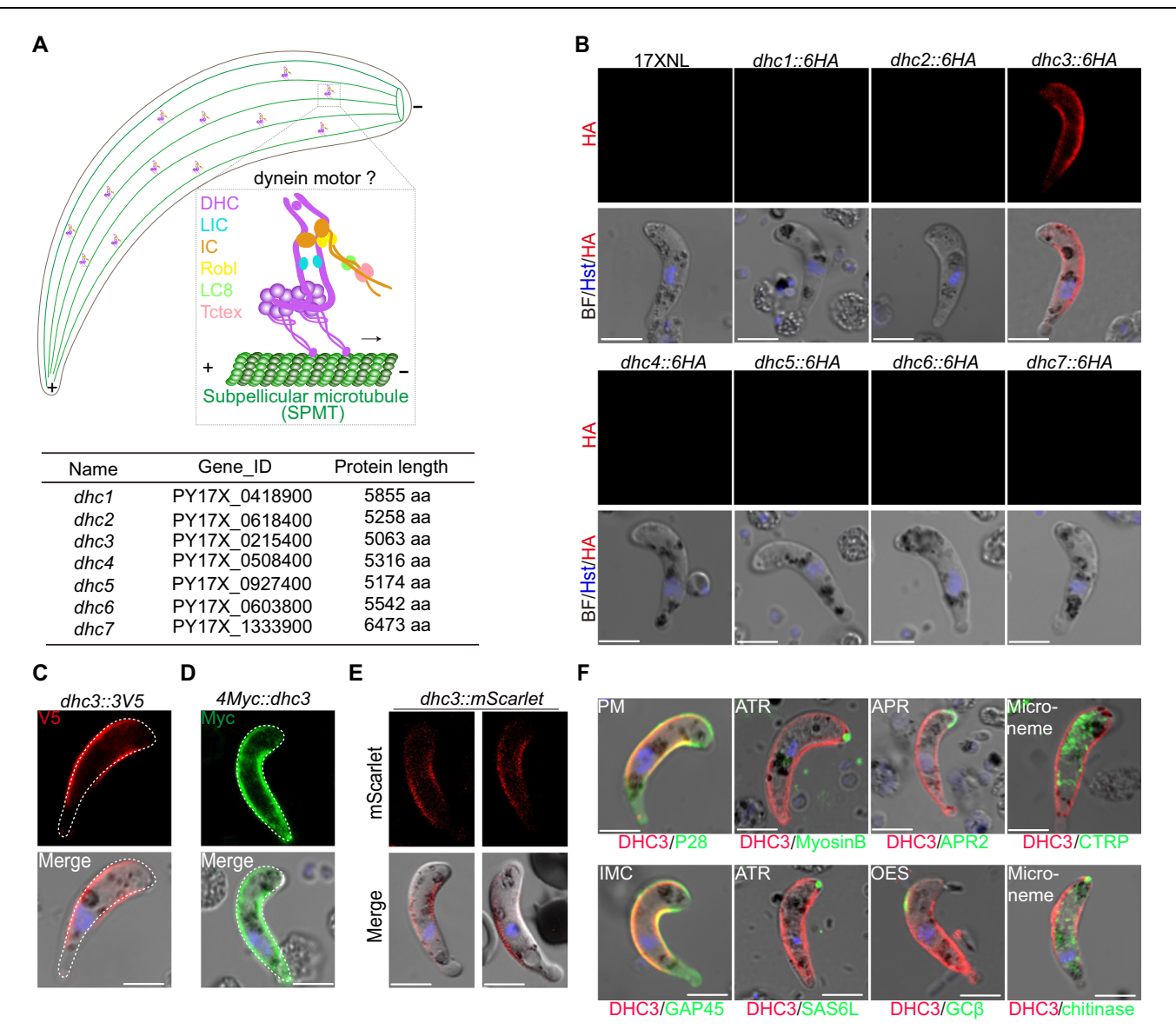


**Fig. 1** | **Protein screening identifies a subpellicular dynein heavy chain DHC3 in ookinetes of** *P. yoelii.* **<b>A** A diagram showing the subpellicular microtubules (SPMTs, green) in the ookinetes and the potential SPMT-based cytoplasmic dynein. The dynein complex is composed of a pair of six different subunits, including one heavy chain (violet), one intermediate chain (orange), one light intermediate chain (cyan), and three light chains (Tctex, pink; Robl, yellow; and LC8, light green). The plus end of the SPMTs is indicated as "+" and the minus end as "–". Seven genes encoding putative dynein heavy chain protein in the *P. yoelii* are shown (lower panel). **B** IFA of seven DHC proteins expression in the ookinetes. Each endogenous protein was C-terminally fused with a 6HA in the *P. yoelii* 17XNL strain and seven modified parasite lines were generated. Hst: DNA dye Hoechst 33342. Three independent experiments. Scale bars: 5 μm. **C** IFA of 3V5-tagged DHC3 in the

ookinetes of the *dhc3::3VS* parasite line. Three independent experiments. Scale bar:  $5 \,\mu m$ . **D** IFA of 4Myc-tagged DHC3 in the ookinetes of the *4Myc::dhc3* parasite line. Three independent experiments. Scale bar:  $5 \,\mu m$ . **E** Fluorescence microscopy observation of mScarlet-tagged DHC3 in living ookinetes of the *dhc3::mScarlet* parasite line. Three independent experiments. Scale bars:  $5 \,\mu m$ . **F** Co-localization analysis by IFA for DHC3 with proteins of known cellular localizations in ookinetes. P28 (plasma membrane, PM), GAP45 (inner membrane complex, IMC), MyosinB and SAS6L (apical tubulin ring, ATR), APR2 (apical polar ring, APR), GC $\beta$  (ookinete extrados site, OES), CTRP and chitinase (microneme) were included. DHC3 was tagged with a 6HA while GC $\beta$ , APR2, SAS6L, and MyosinB were tagged with a 4Myc or 3V5. P28, GAP45, chitinase, and CTRP were detected using the antiserum. Three independent experiments. Scale bars:  $5 \,\mu m$ .

CTRP and chitinase (microneme)<sup>34–36</sup> (Fig. 1F). Among these proteins, P28 and GAP45 showed overlapping signals with DHC3, further supporting the peripheral localization of DHC3 in the ookinetes (Fig. 1F).

# DHC3 associates with SPMTs throughout ookinete morphogenesis

To investigate the localization dynamics of DHC3 during ookinete morphogenesis (see the schematic in Fig. 2A), we collected the parasites in different stages from in vitro *dhc3::6HA* ookinete cultures. IFA showed that DHC3 was distributed in the cytoplasm in the zygote (stage I), moved to the periphery of the protrusion part from stage II to

stage IV, and completely located at the periphery of mature ookinetes (stages V) (Fig. 2A and Fig. S2A). We described the periphery localization level of DHC3 by quantifying fluorescent signals at the periphery over the whole cell (Fig. 2B). DHC3 in the *4Myc::dhc3* parasites displayed similar localization dynamics (Fig. 2A, B). The localization dynamics of DHC3 are similar to that of SPMTs in the ookinete morphogenesis of *P. berghei* and *P. yoelii*<sup>8,13</sup>.

Next, we investigated whether the peripherally localizing DHC3 associates with the SPMTs. First, co-immunostaining of DHC3 (HA tag) and SPMT ( $\alpha$ - and  $\beta$ -Tubulin) in the *dhc3::6HA* parasites detected peripheral co-localization of DHC3 with SPMTs in the protrusion and

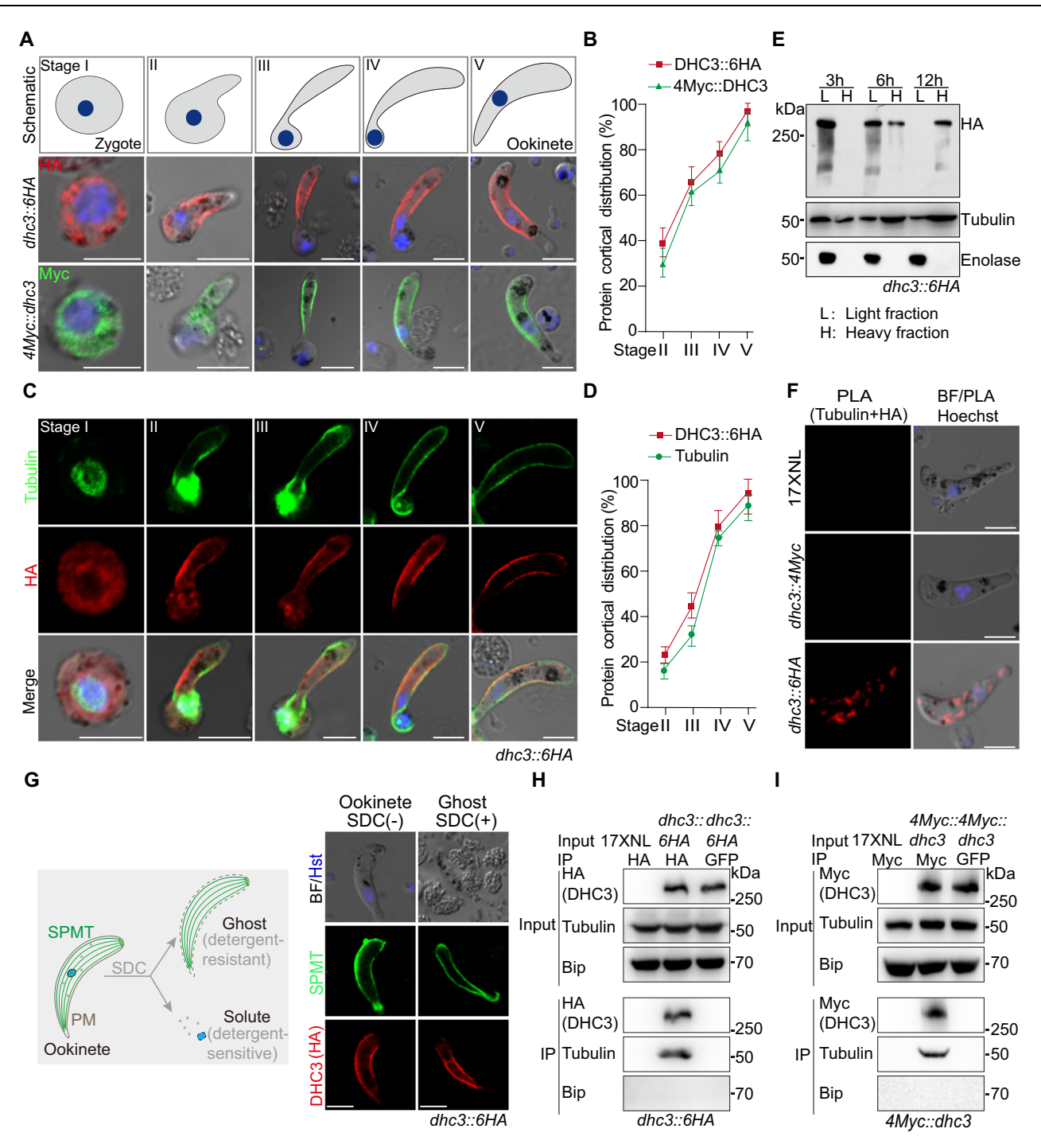


Fig. 2 | DHC3 associates with SPMTs throughout ookinete morphogenesis.

A IFA of DHC3 expression during zygote to ookinete development. A schematic shows the developmental stages (I–V) of ookinete. Two parasite lines dhc3::6HA and 4Myc::dhc3 were analyzed. Three independent experiments. Scale bars: 5 μm. B Protein cortical distribution rate of DHC3 during ookinete development in (A). Values are means  $\pm$  SD (n = 3 biological replicates). C IFA of DHC3 (HA) and SPMTs ( $\alpha$ - and  $\beta$ -Tubulin) during ookinete development of the dhc3::dhA parasites. Three independent experiments. Scale bars: 5 μm. D Protein cortical distribution rate of DHC3 and Tubulin in (C). Values are means  $\pm$  SD (n = 3 biological replicates). E Fractionation analysis of DHC3 in different stages (3, 6, and 12 h) of the dhc3::dhA ookinetes via immunoblot. Light fraction includes cytosolic proteins while heavy fraction includes membrane and cytoskeleton proteins. The cytosolic protein Enolase was used as a loading control. Two independent experiments. F Proximity ligation assay (PLA) detecting protein interaction between DHC3 and SPMTs in the

dhc3::6HA ookinetes. Two independent experiments. Scale bars: 5 μm. **G** SPMT cytoskeleton association analysis of DHC3. The left panel is a diagram showing the isolation procedures of ookinete ghost (SPMTs cytoskeleton) and solute.  $5.0 \times 10^6$  ookinetes were treated with the ionic detergent sodium deoxycholate (SDC), and DHC3 (HA) and SPMTs ( $\alpha$ - and  $\beta$ -Tubulin) were analyzed via IFA in the dhc3::6HA ookinetes and ookinete ghosts. Three independent experiments. Scale bars: 5 μm. **H** SPMTs co-immunoprecipitated with HA-tagged DHC3 in the dhc3::6HA ookinetes. Co-immunoprecipitation was conducted using the anti-HA antibody. BiP as the loading control. Two independent experiments. **1** SPMTs co-immunoprecipitation was conducted using the anti-HA ookinetes. Co-immunoprecipitation was conducted using the anti-Myc antibody. BiP as the loading control. Two independent experiments. Source data are provided as a Source Data file.

elongation processes of ookinetes (Fig. 2C, D). Second, we isolated the heavy fraction (including pellicle membrane and cytoskeleton) and light fraction (including cytoplasm) from the ookinetes extracts of different stages (3, 6, and 12 h) after hypotonic lysis, and showed that DHC3 could be detected in light fraction from early stages, but in heavy fraction of mature ookinetes (Fig. 2E), implying DHC3 association with cytoskeleton in mature ookinetes. Third, proximity ligation assay (PLA), an immunohistochemical method analyzing protein interaction with high specificity and sensitivity<sup>37</sup>, detected PLA signals at the cell periphery of the ookinetes in dhc3::6HA parasites but not in 17XNL and 4Myc::dhc3 parasites when both anti-α-/β-Tubulin and anti-HA antibodies were used (Fig. 2F), indicating proximity between DHC3 and SPMTs. Fourth, we analyzed the association of DHC3 in the ookinete ghost after extraction with the ionic detergent sodium deoxycholate (SDC) (Fig. 2G), which was used for isolating SPMT cytoskeleton in the T. gondii and P. yoelii38,39. In SDC-treated dhc3::6HA ookinetes, the pellicle membranes (PM and IMC) were largely depleted (Fig. S2B). However, DHC3 remained co-localized with SPMTs (Fig. 2G), indicating a close association with ookinete ghost. Fifth, co-immunoprecipitation (Co-IP) with anti-HA or anti-Mvc antibodies indicated that DHC3 binds to Tubulin both in the dhc3::6HA and 4Myc::dhc3 ookinete lysates (Fig. 2H, I). Together, these pieces of evidence indicate that DHC3 associates with SPMTs during ookinete morphogenesis.

We attempted to investigate dynein movement along the SPMTs in living ookinetes of the *dhc3::mScarlet* parasites (Fig. 1E). However, visualization of DHC3::mScarlet moving at the molecular level in the living ookinetes was not successful due to weak signal of endogenous protein and limit in the spatial-temporal resolution of the confocal microscopy. Instead, we used fluorescence recovery after photobleaching (FRAP) and found that the fluorescent signal of DHC3::mScarlet recovered within seconds in the periphery of the *dhc3::mScarlet* ookinetes after photobleaching (Fig. S2C). These results suggested that DHC3 is not localizing in a relatively fixed position at the periphery, consistent with its property as a motor moving dynamically along MT.

# Ultrastructure expansion microscopy (U-ExM) of DHC3 association with SPMTs

To observe the peripheral localization of DHC3 in more detail, the dhc3::6HA ookinetes were physically expanded and imaged using U-ExM<sup>8,13</sup>. Approximately sixty DHC3::6HA-labeled fibers were evenly distributed from the apical to the basal end of the ookinetes (Fig. 3A). A similar localization of 4Myc::DHC3 was observed in the 4Myc::dhc3 ookinetes under U-ExM (Fig. 3B). To further analyze the relative localization of DHC3 in the pellicle, the 4Myc::dhc3 ookinetes were costained with an anti-Myc antibody and protein NHS-ester dye (NHS)<sup>14</sup>. Under U-ExM, 4Myc::DHC3 was closely underneath the apical pellicle indicated by NHS signal in later-stage ookinetes (Fig. S3A). This localization pattern of DHC3 completely resembled the SPMTs distribution in the ookinetes<sup>8,13</sup>. Therefore, we investigated the localization relation of DHC3 and SPMTs in the dhc3::6HA parasites from 3- and 12-h in vitro ookinete culture by U-ExM. The parasites were co-stained with anti- $\alpha$ / β-Tubulin and anti-HA antibodies. In early ookinetes showing minor protrusion, DHC3 overlapped with the initially assembled SPMTs in the apical part, although both DHC3 and α/β-Tubulin were mostly dispersed at the cytoplasm (Fig. 3C and Fig. S3B). DHC3 showed no signal at the nuclear spindle MTs (Fig. 3C). In mature ookinetes, DHC3 was colocalized with SPMTs along their entire length (Fig. 3C, Fig. S3B, C). In addition, detailed images in Fig. 3C showed that the apical tubulin ring (ATR), a compacted structure of MTs at the apex of ookinetes, was not labeled with DHC3. Therefore, DHC3 associates specifically with SPMTs during ookinete development.

The microtubule-binding domain (MTBD), a globular fragment of 80-130 amino acids in the stalk tip, is responsible for the MT binding of DHC<sup>40,41</sup> (Fig. 3D). To further validate the association of DHC3 with SPMTs, we deleted the MTBD and investigated the effect on the SPMT

localization of DHC3. In the P. yoelii, the MTBD (3559-3648 amino acid) is located between the AAA4 and AAA5 of the pseudohexameric ring composed of 6 ATPase modules (Fig. 3D). We used CRISPR-Cas9 to delete the genomic sequences encoding MTBD of DHC3 in the dhc3::6HA parasite and obtained a mutant line designated as  $\Delta MTBD$ . Removal of MTBD had little effect on the protein level of DHC3 in the gametocytes (Fig. 3E), however, *AMTBD* showed reduced formation of mature ookinetes compared to the parental line (Fig. 3F). The truncated DHC3 lost the peripheral localization in the ΔMTBD ookinetes (Fig. 3G). To visualize the DHC3 localization relative to SPMTs at a higher resolution, the parasites were co-stained with antibodies against HA and Tubulin polyglutamylation (PolyE), a marker for the stabilized MT<sup>8,13</sup>. U-ExM indicated that PolyE antibody specifically labeled the apical assembled SPMTs, but not the cytoplasmic Tubulins in early ookinetes of the dhc3::6HA line (Fig. 3H). The MTBD-truncated DHC3 lost SPMT localization and dispersed at the cytoplasm in the early and later stages of ookinetes (Fig. 3H). Therefore, the MTBD contributes to the SPMT binding of DHC3.

#### Component subunits of the SPMT-dynein complex in ookinetes

Cytoplasmic dynein comprises six subunits (Fig. 4A), including one HC, one IC, one LIC, and three LCs (Robl, LC8, and Tctex)<sup>42</sup>. We sought to identify all the subunits of SPMT cytoplasmic dynein in the ookinetes. In the P. yoelii genome, one putative dynein IC gene (PY17X\_0505600), one putative dynein LIC gene (PY17X\_0417700), and 12 putative dynein LC genes are encoded (Fig. S4A). These 14 proteins, conserved in human and rodent Plasmodium species, have not been investigated for expression and localization. We tagged each of these candidate proteins with a 6HA at the C-terminus in the 17XNL using CRISPR-Cas9 and analyzed their expression and localization in ookinetes. IFA of the tagged parasite clones showed that five proteins (LIC, PY17X 0417700; IC, PY17X 0505600; three LCs, PY17X 0505400, PY17X 1431600, and PY17X 0831600) were localized at the periphery of ookinetes (Fig. S4B). In addition, these five proteins displayed similar localization dynamics during ookinete morphogenesis as DHC3 (Fig. S4C) and were not detected in the asexual blood stages (Fig. S4D). To confirm the co-localization of these candidate subunits with DHC3, we engineered parasite clones with each of these five proteins tagged with a 6HA from the 4Myc::dhc3 parasite and obtained five doubletagged parasite lines. Two-colored IFA showed these five proteins were co-localized with DHC3 in the periphery of ookinetes (Fig. 4C). To visualize the association of the protein with SPMTs in more detail, the ookinetes were stained with antibodies against HA and  $\alpha/\beta$ -Tubulin and imaged by U-ExM. These subunits (LIC, IC, Robl, LC8, and Tctex) showed complete co-localization with SPMTs in the ookinetes (Fig. 4D). It is noted that these five subunits showed no signal at the ATR (Fig. 4D), consistent with the results of DHC3. These pieces of evidence indicate that the SPMT-based cytoplasmic dynein complex is composed of DHC3, LIC, IC, and three LCs (Robl, LC8, and Tctex).

# DHC3 is required in ookinete morphogenesis for mosquito midgut infection

To elucidate the function of DHC3 in the life cycle of the parasite, we deleted a 1.0 kb genomic sequence at the coding region (15.3 kb) of *dhc3* in the 17XNL (wild type or WT) using CRISPR-Cas9 (Fig. 5A). The deletion caused a frameshift for the remaining coding sequence. Two independent mutant clones *Adhc3 sc1* and *sc2* were obtained. Both clones exhibited comparable levels of 17XNL in asexual blood stage proliferation (Fig. S5A) and gametocyte formation in mice (Fig. 5B). To evaluate the role of DHC3 in parasite development in mosquitoes, *Anopheles stephensi* mosquitoes were fed on the parasite-infected mice. Both mutant clones produced no midgut oocyst on day 7 post-infection (pi) (Fig. 5C) and no sporozoite in the salivary glands on day 14 pi (Fig. 5D). Consistently no transmission of parasite from mosquitoes to mice was observed (Fig. 5E). To confirm the parasite

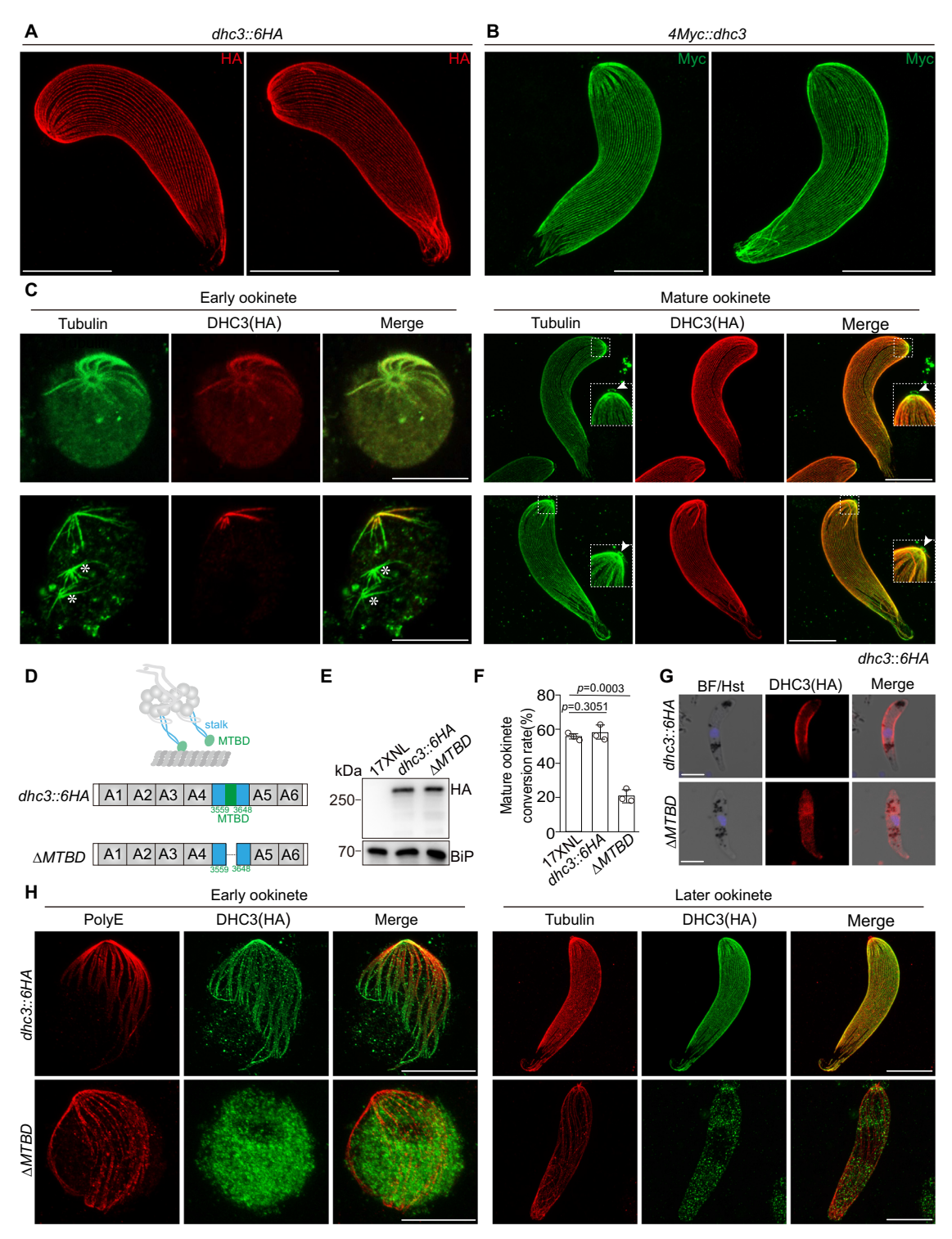


**Fig. 3** | **Ultrastructure expansion microscopy (U-ExM) detecting SPMT association of DHC3.** A U-ExM of DHC3 in the *dhc3::6HA* ookinetes. The parasites were stained with the anti-HA antibody. Three independent experiments with similar results. Scale bars: 5 μm. **B** U-ExM of DHC3 in the *4Myc::dhc3* ookinetes. The parasites were stained with the anti-Myc antibody. Three independent experiments with similar results. Scale bars: 5 μm. **C** U-ExM of DHC3 (HA) and SPMTs ( $\alpha$ - and  $\beta$ -Tubulin) in the early and mature ookinetes of the *dhc3::6HA* parasites. The parasites were co-stained with the anti-HA antibody and anti- $\alpha/\beta$  Tubulin antibodies. White asterisk indicates the spindle while the white arrow indicates the apical tubulin ring (ATR). Three independent experiments with similar results. Scale bars: 5 μm. **D** Diagram showing the microtubule-binding domain (MTBD, green) and truncation of MTBD in DHC3 from the parental parasite *dhc3::6HA*, generating the

modified line  $\Delta MTBD$ . The green number indicates the structural boundary of MTBD. **E** Immunoblot of HA-tagged DHC3 in the gametocytes of the dhc3::6HA and  $\Delta MTBD$  parasites. BiP as a loading control. Two independent experiments with similar results. **F** In vitro ookinete formation of the dhc3::6HA and  $\Delta MTBD$  parasites. Values are means  $\pm$  SEM (n = 3). A two-sided t-test was applied. **G** IFA of DHC3 expression in ookinetes of the dhc3::6HA and  $\Delta MTBD$  parasites. Three independent experiments. Scale bars: 5  $\mu$ m. **H** U-ExM of DHC3 and SPMTs in early stage (left panel) and later-stage ookinetes (right panel) of the dhc3::6HA and  $\Delta MTBD$  parasites. Parasites were co-stained with antibodies against HA and Tubulin polyglutamylation (PolyE). PolyE is a marker for the stabilized MT. Three independent experiments with similar results. Scale bars: 5  $\mu$ m. Source data are provided as a Source Data file.

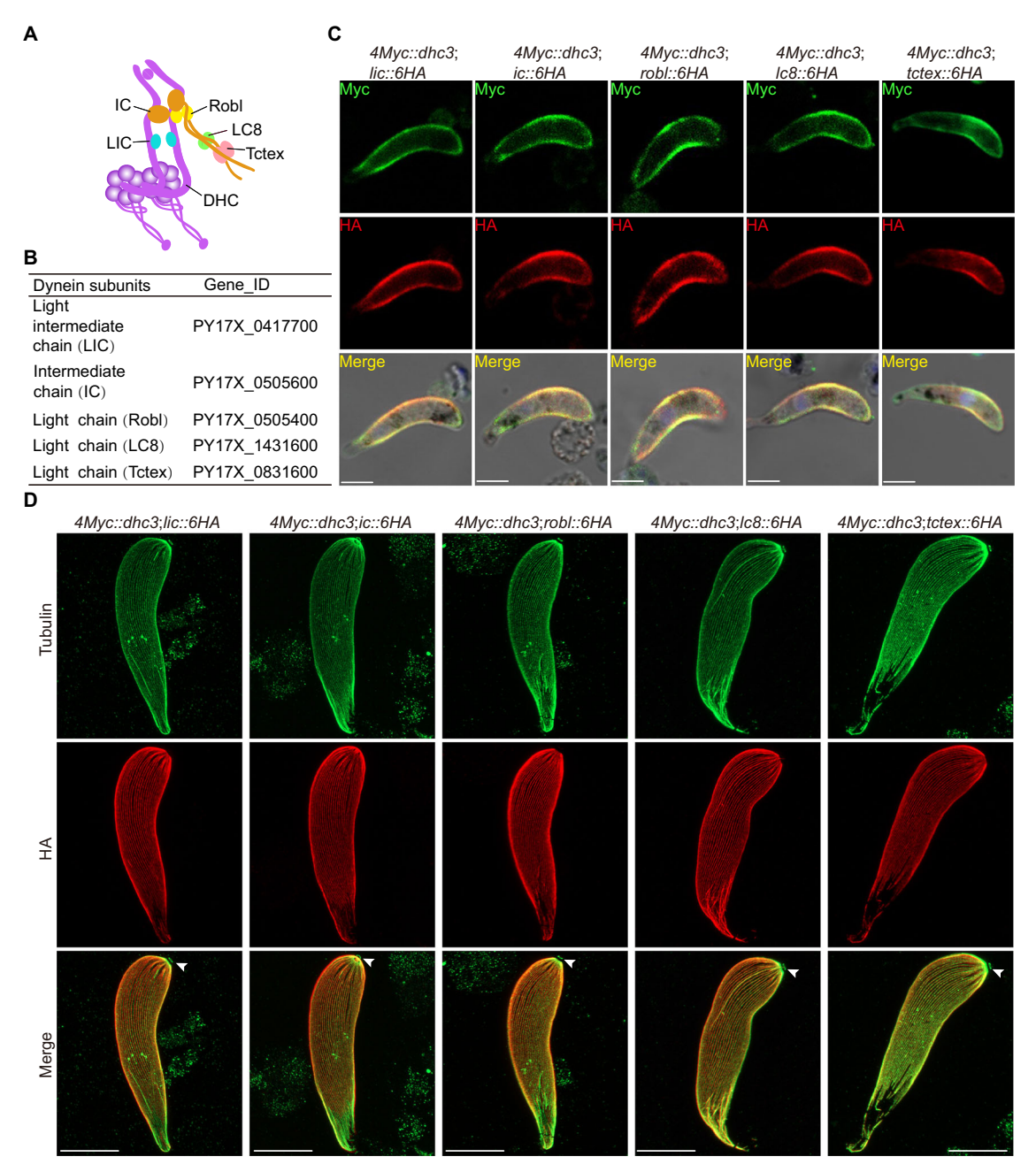


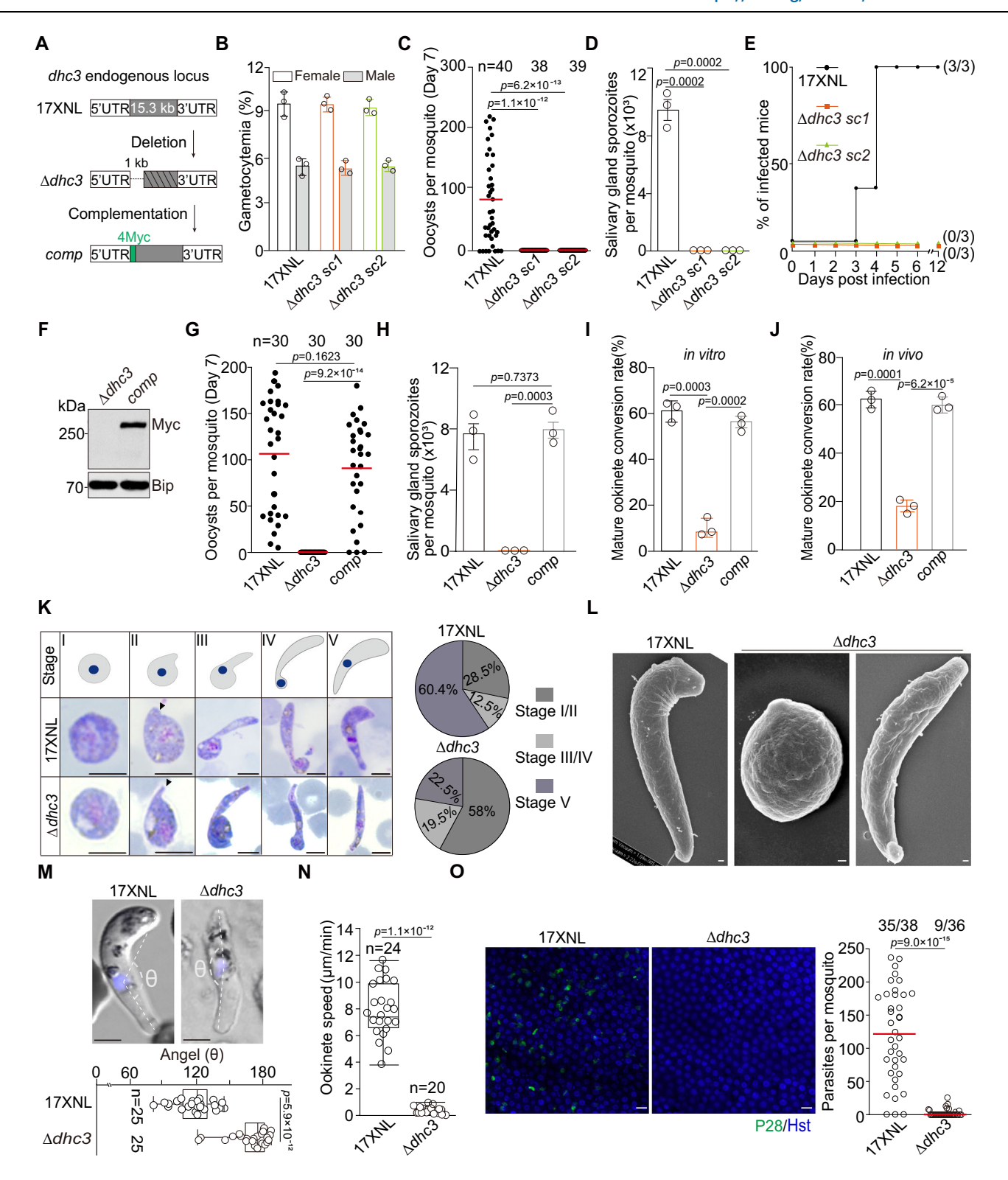
**Fig. 4** | **Identification of SPMT-dynein complex subunits in ookinetes. A** Schematic of the SPMT-dynein complex, composed of six subunits including DHC, LIC, IC, and LCs (Robl, LC8, and Tctex). **B** Information of five genes encoding dynein subunits in the genome of *P. yoelii*. **C** Two-colored IFA of DHC3 with LIC, IC, Robl, LC8, and Tctex in the ookinetes. Each endogenous protein was C-terminally

fused with a 6HA in the *4Myc::dhc3* parasite and five modified lines were generated. Parasites were co-stained with antibodies against HA and Myc. Three independent experiments. Scale bars:  $5\,\mu m$ . **D** U-ExM of SPMTs and five dynein subunits in the ookinete. Parasites were co-stained with antibodies against  $\alpha/\beta$ -Tubulin and HA. White arrow indicates the ATR. Three independent experiments. Scale bars:  $5\,\mu m$ .

transmission defects in mosquitoes were caused by DHC3 deficiency, we introduced the deleted fragment fused with a 4Myc back into the *dhc3* locus of  $\Delta dhc3$  sc1 (Fig. 5A). The complemented line *comp* restored the expression of 4Myc-tagged DHC3 in gametocytes (Fig. 5F) and the formation of oocysts and sporozoites in mosquitoes (Fig. 5G, H).

Next, we delineated the developmental step(s) affected by DHC3 deficiency between gametocyte and oocyst stages. The  $\Delta dhc3$  showed normal gamete formation and fertilization in vitro (Fig. S5B–D) and developed from diploid to tetraploid during ookinete development (Fig. S5E, F). GAP45 staining showed that DHC3 deletion had less effect on the IMC assembly in the  $\Delta dhc3$ -defective ookinetes (Fig. S5G). However, the in vitro assay for zygote to ookinete differentiation

revealed that  $\Delta dhc3$  had a dramatic decrease in ookinete formation (59% in 17XNL, 14% in  $\Delta dhc3$ , and 53% in comp) (Fig. 5I). We isolated ookinetes from infected mosquito midguts and detected similar defects of  $\Delta dhc3$  in vivo (Fig. 5J). Time-course analysis revealed that DHC3 deficiency caused developmental arrestment mainly at stages I and II, and a small proportion of parasites developed into mature-looking ookinetes (Fig. 5K). The defective morphology of the  $\Delta dhc3$  ookinetes was also observed under scanning electron microscopy (SEM) (Fig. 5L). Compared to the 17XNL ookinetes with characteristic crescent shapes, the mature-looking ookinetes of  $\Delta dhc3$  lost cell bending (Fig. 5M). We further assessed the gliding activity of ookinetes in vitro and found that the mature-looking ookinetes of  $\Delta dhc3$  displayed a significantly reduced gliding speed (17XNL:  $8.4 \pm 1.7 \, \mu m/min$ ,



n = 24;  $\Delta dhc3$ : 0.3 ± 0.2 μm/min, n = 20) (Fig. 5N). Since ookinete development, shape, and gliding were impaired, we speculated that the  $\Delta dhc3$  parasites may fail to traverse the mosquito midgut. To test this, the midguts from infected mosquitoes were dissected at 24 hpi and visualized after staining with an antibody against P28 (parasite plasma membrane protein in ookinete and early oocyst). The numbers of P28-positive parasites were significantly reduced in the  $\Delta dhc3$ -infected midguts (parasites per mosquito:  $122 \pm 71$  in 17XNL, n = 38;  $3 \pm 6$  in  $\Delta dhc3$ , n = 36) (Fig. 50). These results demonstrated that DHC3

regulates ookinete development, shape, and gliding for mosquito midgut infection of the parasite.

# Defective apical structures in ookinetes of the DHC3-deficient parasites

The ookinete may use the SPMT-dynein to deliver cargoes from the cell body to the apical distal area for de novo assembly of the IMC, APR, ATR, or micronemes. We therefore investigated the formation of the apical organelles and structures in the ookinetes of the DHC3-deficient

Fig. 5 | DHC3 is required in ookinete morphogenesis for mosquito midgut infection. A Diagram showing genetic deletion and complementation of the dhc3 gene using CRISPR-Cas9. The N-terminus 1.0 kb coding sequence of dhc3 was deleted in the 17XNL strain, generating two mutant clones  $\Delta dhc3$  sc1 and sc2. The Δdhc3 sc1 was complemented by introducing the deleted sequence of the dhc3 gene fusing with an N-terminal 4Myc, generating the complementation clone comp. UTR, untranslated region, B Gametocyte formation in mice. Values are means ± SEM (n = 3 biological replicates). C Midgut oocyst formation in mosquito 7 days post-infection (dpi). n is the number of mosquitoes dissected. Red horizontal lines show the mean value. Two-sided Mann-Whitney U-test. Two independent experiments. D Salivary gland sporozoite formation in mosquito 14 dpi. 30 mosquitoes were counted in each group. Values are means  $\pm$  SEM (n = 3 biological replicates). Two-sided t-test. E Infectivity of sporozoites from mosquito to mice via natural biting. Infected mice were determined by the emergence of the asexual blood-stage parasites. x/y in the bracket is the number of infected mice/total naïve mice used. F Immunoblot of the Myc-tagged DHC3 in gametocytes of the Δdhc3 and comp parasites. Bip as a loading control. Two independent experiments. G Midgut oocysts in mosquitoes infected with the *comp* line 7 dpi. n is the number of mosquitoes. Red horizontal lines show the mean value. Two-sided Mann-Whitney Utest. H Salivary gland sporozoites in mosquitoes infected with the comp line 14 dpi. 30 mosquitoes were counted in each group. Values are means  $\pm$  SEM (n=3 biological replicates). Two-sided t-test. I Ookinete formation in vitro. Values are means  $\pm$  SEM (n = 3 biological replicates). Two-sided t-test. J Ookinete formation in

the midgut of infected mosquitoes. Values are means  $\pm$  SEM (n = 3 biological replicates). Two-sided t-test. K Giemsa staining of cultured ookinetes. The upper diagram indicates morphological changes from zygote to ookinete. The black arrow indicates the apical. Scale bars: 5 µm. The pie chart shows the percentage of different subtypes within the ookinete population. Three independent experiments with similar results. L Representative images from scanning electron microscopy of 17XNL and  $\Delta dhc3$  ookinetes. Scale bars: 200 nm. Three independent experiments with similar results. M Ookinete cell shape. The nucleus center point was set as a vertex of the angel  $(\theta)$  from two lines of nucleus-apical and nucleus-basal for each ookinete. n is the number of ookinetes. Scale bars: 5  $\mu$ m. The lower panel is the data quantification. Box plot: center line = median, box range 25th-75th percentile, minimum/maximum denoted by whiskers. Two-sided Mann-Whitney U-test. Two independent experiments. N Ookinete gliding motility using the in vitro Matrigelbased assay. n is the number of ookinetes. Box plot: center line = median, box range 25th-75th percentile, minimum/maximum denoted by whiskers. Two-sided Mann-Whitney *U*-test. Two independent experiments. **O** IFA of P28 in mosquito midguts infected with 17XNL and  $\Delta dhc3$  24 hpi. P28 is a plasma membrane protein of ookinete and early oocyst. Scale bars: 10 µm. The right panel shows the quantification of parasites per mosquito midgut. x/y on the top is the count of midguts containing parasites/the count of midguts measured. Red horizontal lines show the mean value. Two-sided Mann-Whitney *U*-test. Two independent experiments. Source data are provided as a Source Data file.

parasites. Transmission electron microscopy (TEM) revealed an aberrant apical part in early- and later-arrested ookinetes of Δdhc3 compared to 17XNL. Intact IMC at the apical pellicle was detected underlying the plasma membrane in both 17XNL and Δdhc3 ookinetes (Fig. 6A and Fig. S6), which is consistent with ookinete staining with GAP45 in Fig. S5G. These results suggest that DHC3 disruption had little effect on the IMC formation. In TEM micrographs of 17XNL ookinetes, APR is adjoined with apical IMC (Fig. 6A and Fig. S6). However, APR appeared posteriorly at a distance from the apical IMC in the  $\Delta dhc3$  ookinetes (Fig. 6A and Fig. S6), suggesting APR detachment from the apical IMC. In addition, the detached APR appeared structurally defective (Fig. 6A and Fig. S6). U-ExM analysis of ookinetes after staining with NHS-ester dve also revealed the impaired APR in the  $\Delta dhc3$  ookinetes (Fig. S7A). To visualize the defects of APR in more detail, we deleted the dhc3 gene in two parasite lines apr2::4Myc and ara1::4Myc<sup>13</sup>, in which the APR proteins APR2 and ARA1 were tagged with a 4Myc. In both mutant parasites apr2::4Myc;\(\Delta\)dhc3 and ara1::4Myc;\(\Delta\)dhc3, most of the defected ookinetes retained the apical localization of APR2 and ARA1. However, the IFA signals of APR2 (Fig. 6B, C) and ARA1 (Fig. 6D, E) were decreased in the ookinetes of the mutant compared to the parental line (Fig. 6C, E). U-ExM further confirmed the impaired APR in the later-arrested ookinetes of apr2::4Myc;Δdhc3 (Fig. S7B).

Detailed images of TEM revealed that the apical tubulin ring (ATR), an MT structure at the apical extremity of ookinetes, was not detected in early- and later-arrested ookinetes of  $\Delta dhc3$  compared to 17XNL (Fig. 6A and Fig. S6). U-ExM confirmed the absence of ATR in the  $\Delta dhc3$  ookinetes after  $\alpha/\beta$ -Tubulin staining (Fig. 6F). To further test this, we deleted the dhc3 gene in the parasite line  $myosinb::4Myc^{13}$ , in which the ATR-localizing protein MyosinB was tagged with a 4Myc. Apical localization of MyosinB was lost in defective ookinetes of the mutant  $myosinb::4Myc;\Delta dhc3$  compared to the parental line (Fig. 6G), which is consistent with the results of TEM and U-ExM.

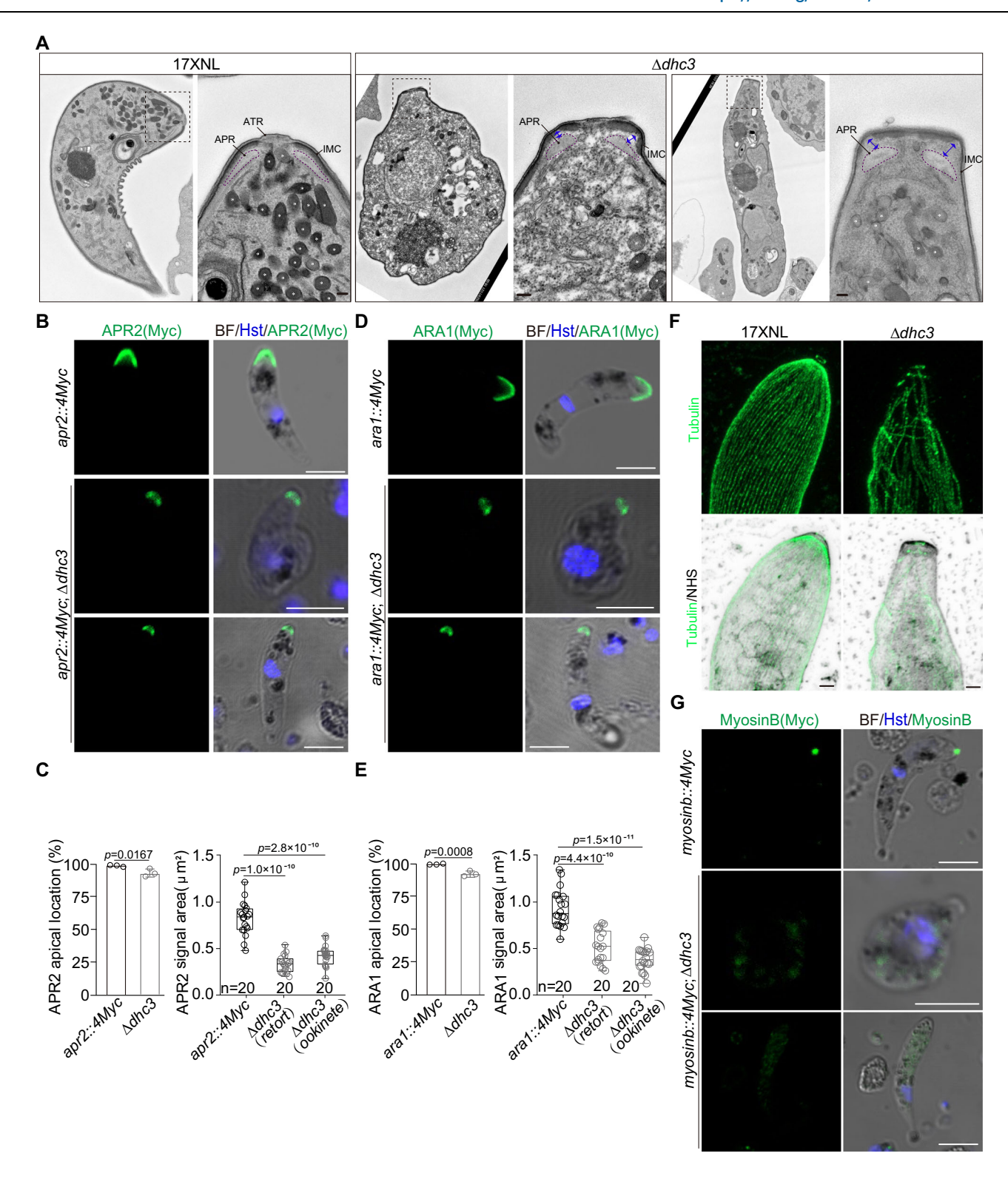
ExM images of  $\alpha/\beta$ -Tubulin in Fig. 6F also detected defects of apical SPMTs, many of which lost cortical attachment and were disorderly scattered in the  $\Delta dhc3$  ookinetes. Disturbed pellicle attachment of apical SPMTs may result from the impaired APR, which directs the assembly of SPMTs and stabilizes the SPMTs in the ookinetes<sup>13</sup>. Consistently, we noticed a marked decrease of apical micronemes in ookinetes of the  $\Delta dhc3$  compared to 17XNL, where most of the micronemes are apically localized (Fig. 6A, Figs. S6 and S7C). We analyzed the microneme protein secretion by immunoblot and found that the microneme-secreted proteins CTRP,

chitinase, and WARP were reduced in the ookinete culture supernatants of  $\Delta dhc3$  compared to 17XNL (Fig. S7D, E). Therefore, DHC3 disruption also affects the apical formation or localization of SPMTs and micronemes

# Small GTPases Rab11A and Rab11B co-localize and interact with DHC3

Small GTPases of the Rab family participate in cargo transport via vesicle trafficking in the eukaryotes<sup>43,44</sup>. A recent study demonstrated the essential role of Rab11A in the *P. berghei* ookinete development<sup>45</sup>. Knockdown of rab11a via promoter swap strategy inhibited ookinete development, and most of the ookinetes failed to elongate after protrusion<sup>45</sup>. The Rab11A-deficient defects resembled the phenotype of the DHC3 null parasite, prompting us to explore the potential association between Rab proteins and DHC3 in ookinete development (Fig. 7A). Plasmodium encodes eleven Rab proteins. Among them, Rab1A, Rab7, Rab11A, Rab11B, and Rab18 displayed relatively high levels of transcripts in gametocytes from previous transcriptome profiles<sup>46</sup> (Fig. 7B). We investigated the expression and localization of these five Rab proteins in the ookinetes. Since the C-terminal modification of Rab would inactivate the protein<sup>47</sup>, we failed to tag the endogenous protein at the C-terminus after several attempts. Alternatively, the expression cassettes of rab genes were integrated into the p230p locus using CRISPR-Cas9 in the dhc3::6HA parasite for transgenic overexpression. Each gene was tagged with a 4Myc at the N-terminus and driven by the hsp70 5'-UTR and the dhfr 3'-UTR. Five double-tagged parasite lines (dhc3::6HA;4Myc::rab1a, dhc3::6HA;4Myc::rab7, dhc3::6HA;4Myc::rab11a, dhc3::6HA;4Myc::rab11b, dhc3::6HA;4Myc::rab18) were obtained (Fig. 7C). IFA showed that Rab11A and Rab11B were primarily distributed at the periphery and colocalized with DHC3 in ookinetes of the dhc3::6HA;4Myc::rab11a (DTS1) and dhc3::6HA;4Myc::rab11b (DTS2) lines, respectively (Fig. 7C). Rab1A, Rab7, and Rab18 appeared to be cytoplasmic (Fig. 7C). Rab11A localization is in agreement with that of Rab11A detected by antiserum in the P. berghei ookinete<sup>45</sup>. Time-course analysis of ookinete development showed that Rab11A and Rab11B displayed similar localization patterns as DHC3 (Fig. S8A, B).

Peripheral co-localization with DHC3 suggested that Rab11A and Rab11B associate with dynein along the SPMTs. Consistent with this, U-ExM observed co-localization of Rab11A and Rab11B with SPMTs in mature ookinetes after staining with anti- $\alpha/\beta$ -Tubulin and anti-Myc antibodies (Fig. 7D). Detailed images also showed that



Rab11A and Rab11B had no signal at the ATR (Fig. 7D), similar to the subunits of dynein shown in Figs. 3C and 4D. Co-IP using the anti-Myc antibody detected the interaction between DHC3 and Rab11A in the ookinete lysates of the *DTS1* line (Fig. 7E). Similarly, the Co-IP interaction between DHC3 and Rab11B was observed in the *DTS2* ookinetes using anti-Myc or anti-HA antibodies respectively (Fig. 7F, G). These results demonstrated that Rab11A and Rab11B are associated with the DHC3-residing dynein which tracks along the SPMTs (Fig. 7A).

# GTPase activity is necessary for Rab11A and Rab11B colocalization with DHC3

We next tested whether Rab11A and Rab11B co-localization with DHC3 requires the GTPase activity. Mutation in the GTPase domain at residue 25 from serine to asparagine (S25N) had been shown to stabilize the protein in a dominant-negative (DN) GDP-bound state of Rab11A, while point mutation of residue 71 from glutamine to leucine (Q71L) resulted in the constitutively active (CA) GTP-bound state<sup>48,49</sup>. The expression cassettes of Rab11A-DN (harboring S25N) and Rab11A-CA (harboring

#### Fig. 6 | Defective apical structures in ookinetes of the DHC3-deficient parasites.

A Representative images from transmission electron microscopy (TEM) of 17XNL and  $\Delta dhc3$  ookinetes. The apical area (black dashed box) is zoomed in. The apical polar ring (APR), apical tubulin ring (ATR), and inner membrane complex (IMC) are indicated. APR is adjoined with apical IMC in the 17XNL ookinete while a gap (blue arrow) appears between apical IMC and APR in both early and later-stage defective ookinetes of  $\Delta dhc3$ . Micronemes were labeled with an asterisk. Scale bars: 200 nm. Three independent experiments. **B** IFA of Myc-tagged APR2 in apr2::4Myc and apr2::4Myc;  $\Delta dhc3$  ookinetes. The dhc3 gene was deleted in the apr2::4Myc parasite in which the APR protein APR2 was tagged with a 4Myc. Scale bars: 5  $\mu$ m. Three independent experiments. **C** Quantification of APR2 signal in (**B**). Left panel shows the percentage of ookinetes with APR2 apical localization. 100 cells were analyzed in each group of each replicate. Values are means  $\pm$  SEM (n=3 biological replicates). Two-sided t-test. The right panel shows the IFA signal area of APR2. 20 cells were analyzed in each group. Box plot: center line = median, box range 25th–75th percentile, minimum/maximum denoted by whiskers. Two-sided Mann–Whitney U-

test. **D** IFA of Myc-tagged ARA1 in the *ara1::4Myc* and *ara1::4Myc*;∆*dhc3* ookinetes. The dhc3 gene was deleted in the ara1::4Myc parasite line in which the APR protein ARA1 was tagged with a 4Myc. Scale bars: 5 µm. Three independent experiments. **E** Quantification of ARA1 signal in (**D**). Left panel shows the percentage of ookinetes with ARA1 apical localization. 120 cells were analyzed in each group of each replicate. Values are means  $\pm$  SEM (n = 3 biological replicates). Two-sided t-test. The right panel shows the IFA signal area of ARA1. 20 cells were analyzed in each group. Box plot: center line = median, box range 25th-75th percentile, minimum/maximum denoted by whiskers. Two-sided Mann-Whitney U-test. F U-ExM of SPMTs in the 17XNL and  $\Delta dhc3$  ookinetes. Parasites were co-stained with the NHS-ester dye and antibodies against α-/β-Tubulin. Scale bars: 5 μm. Three independent experiments. G IFA of Myc-tagged MyosinB in the myosinb::4Myc and myosinb::4Mvc:Δdhc3 ookinetes. The dhc3 gene was deleted in the myosinb::4Mvc parasite line in which the ATR protein MyosinB was tagged with a 4Myc. Scale bars: 5 μm. Three independent experiments. Source data are provided as a Source Data file.

Q71L) were integrated into the *p230p* locus of the *dhc3::6HA* parasite using CRISPR-Cas9 (Fig. 8A). Both proteins were tagged with a 4Myc at the N-terminus and driven by the promoter of gene isp1 for ectopic expression in the ookinetes. Immunoblot confirmed that Rab11A-CA and Rab11A-DN were expressed in the ookinetes, but not in the asexual blood stages (Fig. 8B). Co-IP detected the interaction of DHC3 with Rab11A-WT and Rab11A-CA, but not with Rab11A-DN in the ookinete lysates (Fig. 8C). Consistent with the Co-IP results, U-ExM revealed that Rab11A-DN lost SPMT localization in the defective ookinetes, while Rab11A-CA behaved like Rab11A-WT (Fig. 8D). Using a similar strategy, we overexpressed the Rab11B-DN (harboring T23N) and Rab11B-CA (harboring Q69L) in the ookinetes of the dhc3::6HA parasite (Fig. 8E, F). Rab11B-DN lost both DHC3 interaction and SPMT localization, while Rab11B-CA behaved like Rab11B-WT (Fig. 8G, H). Therefore, Rab11A and Rab11B require the GTPase activity for DHC3 interaction and SPMT localization.

# Localization of Rab11A and Rab11B to SPMTs requires DHC3 but not vice versa

To investigate whether SPMT localization of Rab11A and Rab11B is dependent on DHC3, we deleted the *dhc3* gene in the *dhc3::6HA;4-Myc::rab11a* (*DTS1*) and *dhc3::6HA;4Myc::rab11b* (*DTS2*) parasites, generating two mutant lines *DTS1;Δdhc3* and *DTS2;Δdhc3*. DHC3 depletion did not affect the protein amount of Rab11A and Rab11B in either gametocytes or early ookinetes (Fig. S8C, D), ruling out an effect of DHC3 on protein synthesis of Rab11A and Rab11B. To visualize the Rab localization relative to SPMTs in early ookinetes at a higher resolution, the parasites were co-stained with antibodies against Myc and PolyE. U-ExM indicated that in the absence of DHC3, Rab11A lost SPMT localization and was dispersed in the cytoplasm in early ookinetes of the *DTS1;Δdhc3* parasite (Fig. 9A). Similar to Rab11A, Rab11B lost SPMT localization in the early ookinetes of the *DTS2;Δdhc3* parasite compared to the parental line *DTS2* (Fig. 9B).

We next investigated whether Rab11A and Rab11B influence the SPMT localization of DHC3. Several attempts to disrupt the *rab11a* or *rab11b* gene failed in the *P. yoelii* parasite, suggesting an essential role in the asexual blood stage. The essential nature of Rab11A is consistent with results in recent studies of Rab11A in *P. berghei* and *P. falciparum*<sup>45,50</sup>. Overexpression of the dominant-negative (DN) mutant protein has been utilized to interfere with the endogenous Rab function in many organisms, including *T. gondii*<sup>51</sup>. We analyzed the *dhc3::6HA* parasites with overexpressed dominant-negative (DN) and constitutively active (CA) Rab11A respectively, and measured the localization of DHC3. In the presence of Rab11A-CA, DHC3 was colocalized with the apical SPMTs stained by PolyE in early ookinetes of the *dhc3::6HA;rab11a-CA* parasite under U-ExM (Fig. 9C). Notably, DN inhibition of Rab11A had less effect on the SPMT localization of DHC3 in the *dhc3::6HA;rab11a-DN* early ookinetes (Fig. 9C). Using the

similarly designed Rab11B-DN (harboring T23N) and Rab11B-CA (harboring Q69L), we found that DN inhibition of Rab11B also had less effect on the SPMT localization of DHC3 (Fig. 9D). Together, SPMT localization of Rab11A and Rab11B requires DHC3 while SPMT tracking of DHC3 requires neither Rab11A nor Rab11B. These results of protein localization dependency are in agreement with the relative position of proteins in the "Cargo-Rab-Dynein-MT" model (Fig. 9E).

# Disturbing Rab11A or Rab11B phenocopies DHC3 deficiency in ookinete morphogenesis

We analyzed the development and transmission of the dhc3::6HA;rab11a-DN and dhc3::6HA;rab11b-DN parasites. DN inhibition of Rab11A in ookinetes had less effect on the parasite asexual blood stage proliferation and gametocyte formation in mice (Fig. 10A, B). However, the dhc3::6HA;rab11a-DN parasite displayed a dramatic decrease in ookinete formation both in the in vitro culture (Fig. 10C) and in the infected mosquito midguts (Fig. 10D). We further analyzed the midgut transversal of ookinetes and found that the number of ookinetes and early oocysts (P28-positive) was reduced in the dhc3::6HA;rab11a-DN-infected mosquito midguts dissected at 24 hpi (Fig. 10E). Consistent with the defects in ookinete formation and midgut transversal, the dhc3::6HA;rab11a-DN parasite produced no midgut oocyst on day 7 pi (Fig. 10F) and no sporozoite in the salivary glands on day 14 pi (Fig. 10G). In the parallel test, DN inhibition of Rab11B resulted in defects in the ookinete formation and mosquito transmission of the dhc3::6HA;rab11b-DN parasite (Fig. 10H-N), similar to dhc3::6HA;rab11a-DN parasite. Thus, DN inhibition of Rab11A or Rab11B phenotypically mimics DHC3 deficiency in ookinete morphogenesis and mosquito midgut infection of parasites.

# **Discussion**

In *Plasmodium*, the cytoskeleton of SPMTs plays a mechanical role in supporting cell shape and rigidity of the invasive zoite stages<sup>4,9</sup>. For ookinete development, the parasite undergoes massive expansion of the plasma membrane and acquires a complete set of apical organelles and structures via de novo assembly. Thus, intracellular cargo trafficking appears essential for ookinete growth. Indeed, SPMTs are also proposed to function as the tracks for retrograde motor-driven intracellular cargo transport in ookinetes. However, the SPMT-based protein motor has not been identified. In this study, we identified the SPMT-based cytoplasmic dynein complex, in which the mechanical force-producing subunit DHC3 is essential for ookinete morphogenesis, shape, and gliding motility. In addition, we found two small GTPase proteins Rab11A and Rab11B as possible cargo receptors between the SPMT-dynein and as-yet uncharacterized intracellular cargoes. This study reveals a dynein-Rab11A/ Rab11B machinery for intracellular cargo transport in ookinete morphogenesis.

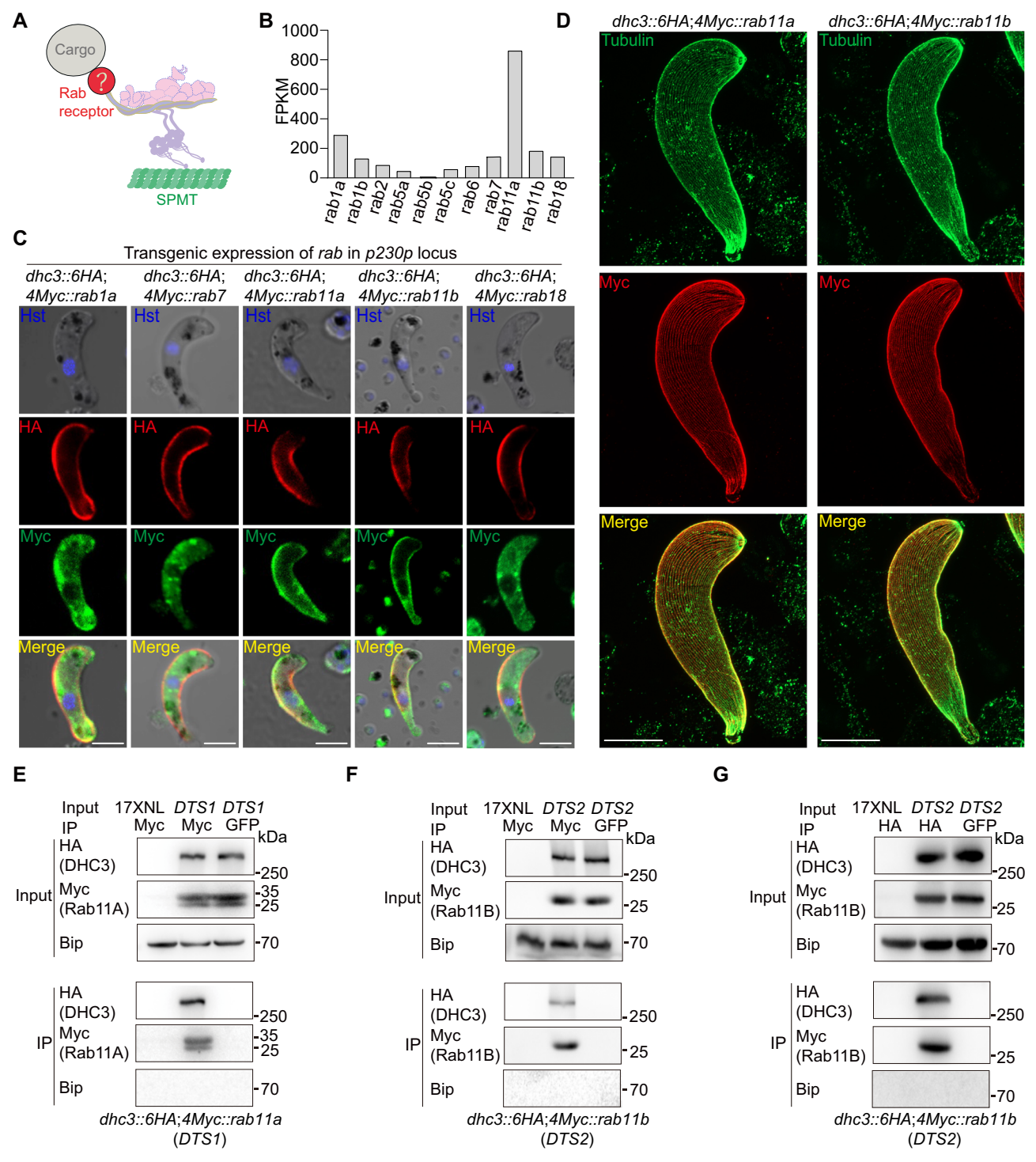


**Fig. 7** | **Two small GTPase Rab11A and Rab11B co-localize and interact with DHC3. A** Diagram showing the potential Rab protein as a cargo receptor linking dynein and cargo. **B** Eleven Rab genes in the *Plasmodium* and their transcript level in the gametocyte of *P. berghei*. Rab1A, Rab7, Rab11A, Rab11B, and Rab18 show relatively high transcript levels. The data comes from the published transcriptomes by Otto, T.D. 2014. **C** Co-localization analysis of DHC3 with Rab1A, Rab7, Rab11A, Rab11B, and Rab18 in ookinetes. The expression cassette of each *rab* gene was integrated into the *p230p* locus in the *dhc3::6HA* parasite for overexpression. Each gene was tagged with a 4Myc at the N-terminus and driven by the *hsp70* S′-UTR and the *dhfr* 3′-UTR. Five double-tagged parasite lines were obtained and co-stained with antibodies against HA and Myc. Scale bars: 5 μm. Three independent experiments. **D** U-ExM of Rab11A and Rab11B association with SPMTs in

ookinetes of two double-tagged parasite lines *dhc3::6HA;4Myc::rab11a* and *dhc3::6HA;4Myc::rab11b*. Parasites were co-stained with antibodies against α/β-Tubulin and Myc. Scale bars: 5 μm. Three independent experiments. **E** Myc-tagged Rab11A co-immunoprecipitated with the HA-tagged DHC3 in the *dhc3::6HA;4My-c::rab11a* (*DTS1*) ookinetes. The anti-Myc antibody was used for immunoprecipitation. BiP as the loading control. Three independent experiments. **F** Myc-tagged Rab11B co-immunoprecipitated with the HA-tagged DHC3 in the *dhc3::6HA;4My-c::rab11b* (*DTS2*) ookinetes. The anti-Myc antibody was used for immunoprecipitation. Three independent experiments. **G** HA-tagged DHC3 co-immunoprecipitated with the Myc-tagged Rab11B in the *DTS2* ookinetes. The anti-HA antibody was used for immunoprecipitation. Three independent experiments. Source data are provided as a Source Data file.

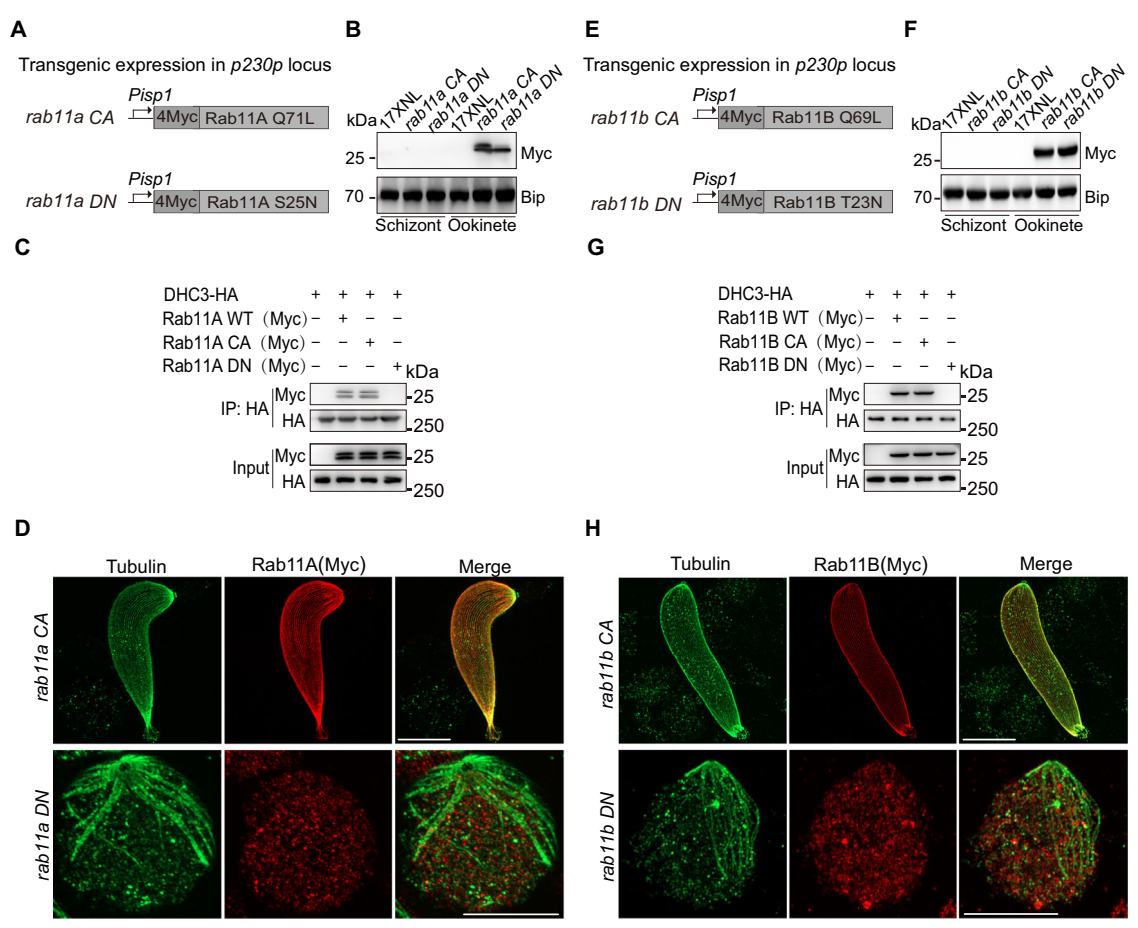
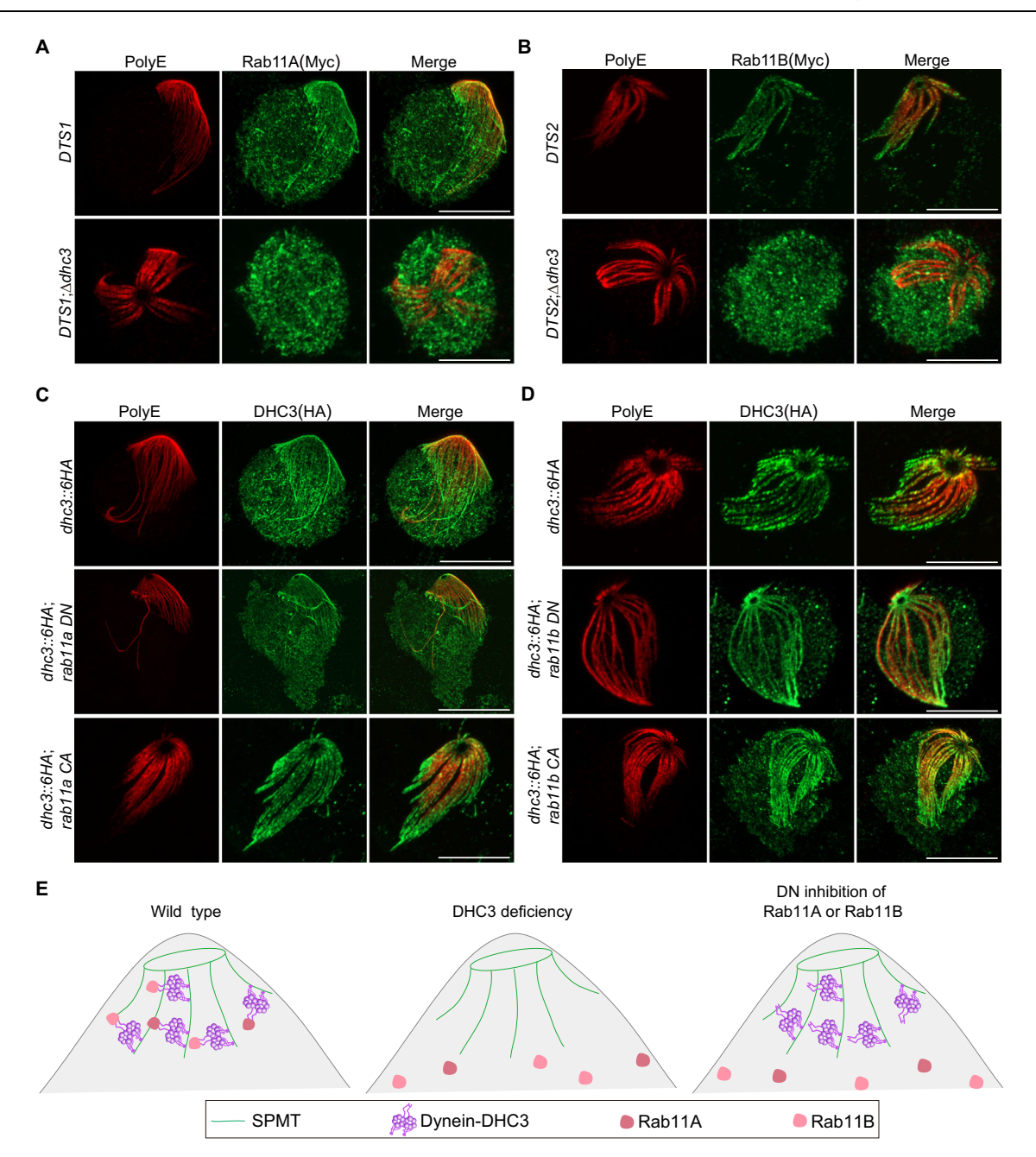


Fig. 8 | GTPase activity is necessary for Rab11A and Rab11B co-localization with DHC3. A Diagram of the expression cassettes of Rab11A-CA (Q71L mutation causing a constitutively active statue of Rab11A) and Rab11A-DN (S25N mutation causing a dominant-negative statue of Rab11A) for overexpression in the ookinetes. Each gene was tagged with a 4Myc at the N-terminus, driven by the promoter of the gene isp1, and integrated into the p230p locus in the dhc3::6HA parasite. B Immunoblot of Myc-tagged Rab11A-CA and Rab11A-DN expression in the schizont and ookinete. BiP as a loading control. Three independent experiments. C HA-tagged DHC3 co-immunoprecipitated with the Myc-tagged Rab11A-WT and Rab11A-CA, but not with Rab11A-DN in ookinetes. Three independent experiments. D Co-localization analysis of Rab11A-CA and Rab11A-DN with SPMTs in ookinetes by U-ExM. Parasites were co-stained with antibodies against  $\alpha/\beta$ -Tubulin and Myc. Scale bars: 5 μm. Three independent experiments. E Diagram of the expression

cassettes of Rab11B-CA (Q69L mutation causing a constitutively active statue of Rab11B) and Rab11B-DN (T23N mutation causing a dominant-negative statue of Rab11B) for overexpression in the ookinetes. Each gene was tagged with a 4Myc at the N-terminus, driven by the promoter of the gene isp1, and integrated into the p230p locus in the dhc3::6HA parasite. F Immunoblot of Myc-tagged Rab11B-CA and Rab11B-DN expression in the schizont and ookinete. Three independent experiments. G HA-tagged DHC3 co-immunoprecipitated with the Myc-tagged Rab11B-WT and Rab11B-CA, but not with Rab11B-DN in ookinetes. Three independent experiments. H Co-localization analysis of Rab11B-CA and Rab11B-DN with SPMTs in ookinetes by U-ExM. Parasites were co-stained with antibodies against  $\alpha/\beta$ -Tubulin and Myc. Scale bars:  $5\,\mu$ m. Three independent experiments. Source data are provided as a Source Data file.

Cytoplasmic dynein-1 (referred to as cytoplasmic dynein) is a major type of dynein motor that drives the movement of intracellular cargo toward the minus ends of MTs<sup>52</sup>. The dynein family also includes the axonemal dynein for ciliary or flagellar beating and the IFT dynein (known as cytoplasmic dynein-2) which drives intraflagellar transport on the axoneme<sup>27</sup>. Cytoplasmic dynein is a structurally conserved 1.6-MDa complex composed of a homodimer of DHC and several pairs of smaller noncatalytic subunits, including one IC, one LIC, and three LCs<sup>42</sup>. The *Plasmodium* genome encodes a total of 7 putative DHC proteins (DHC1 to DHC7), but it is so far unclear which are cytoplasmic or axonemal. We analyzed the expression and localization of all 7 DHC proteins of P. yoelii and found only DHC3 expressed in ookinetes and distributed along the ookinete periphery (Fig. 1B-E). This is consistent with the observation that one cytoplasmic DHC protein evolves in eukaryotes<sup>28</sup>. Using homology search and localization validation, other dynein subunits (LIC, IC, Robl, LC8, and Tctex) were identified and showed similar peripheral localization in the ookinetes (Fig. 4C). U-ExM further detected the co-localization between SPMT and all these six subunits of dynein in ookinetes. Importantly, the cytoplasmic dynein bound the SPMTs after SPMT biogenesis from the early stage of ookinete development.

We initially thought that *Plasmodium*'s SPMT cytoplasmic dynein may exist in all three SPMT-containing zoite stages (merozoite, ookinete, and sporozoite). Surprisingly, DHC3 was detected only in the ookinetes and sporozoites but not in the merozoites (Fig. S1A). The lack of SPMT-based cytoplasmic dynein in the merozoites was further confirmed as no expression of the other dynein subunits (LIC, IC, and three LCs) was detected in the asexual blood stages (Fig. S4D). These results imply no existence of the SPMT-based and cytoplasmic dyneindriven cargo transport in the merozoite. Why does the SPMT-based cytoplasmic dynein exist in the ookinete but not in the merozoite? In erythrocytic schizogony for merozoite formation, the cortex membranes invaginate and engulf the cellular contents, forming the daughter merozoites<sup>53,54</sup>. In contrast, the zygote undergoes massive expansion of the plasma and cortex membranes for ookinete growth. Merozoite formation hence displays a mode of inward invagination inside the mother schizont, which is different from the ookinete outward budding from the zygote. For merozoite, the actin filament-based



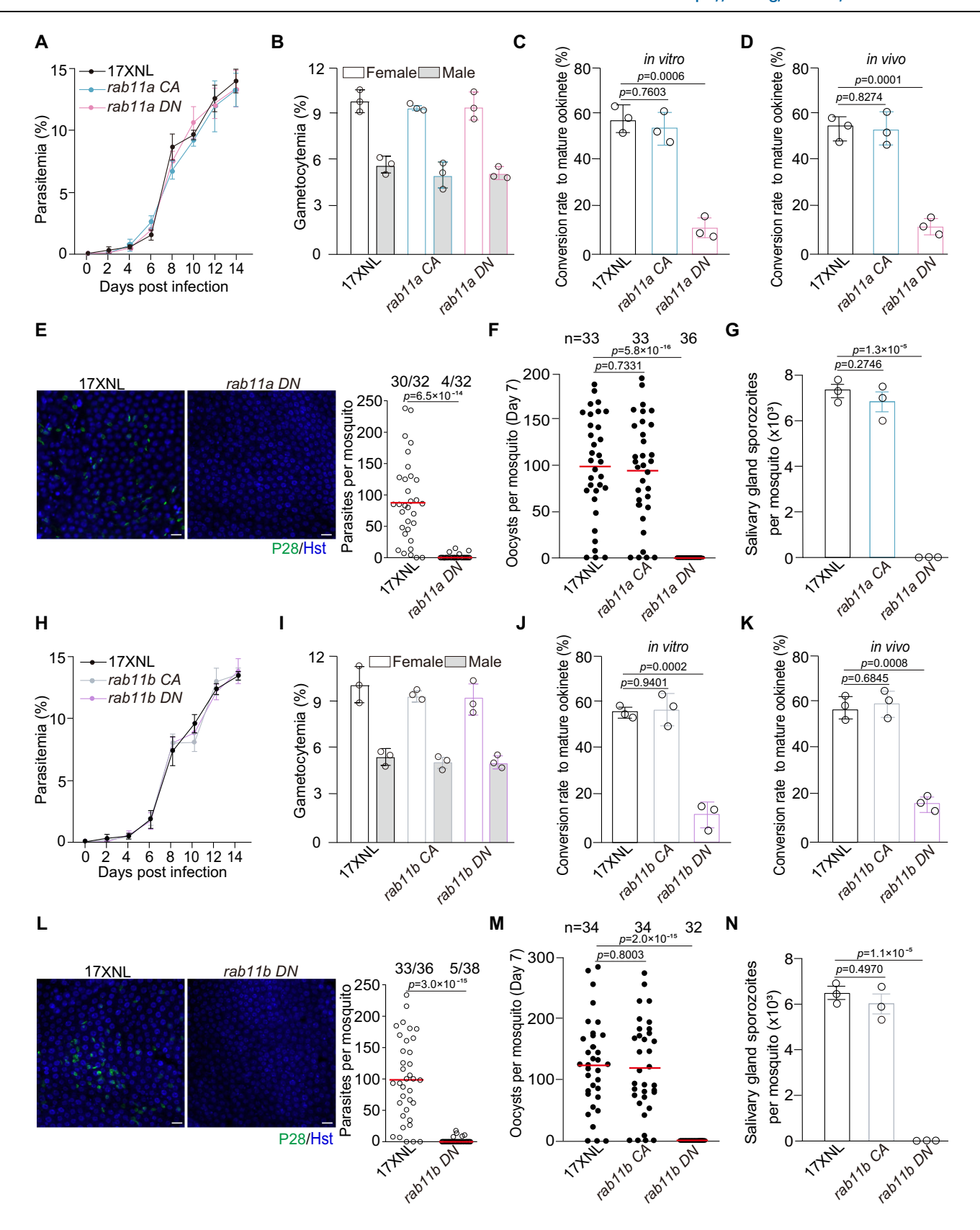
**Fig. 9** | **Localization of Rab11A and Rab11B to SPMTs requires DHC3 but not vice versa.** A U-ExM of SPMTs and Rab11A in early ookinetes of the *dhc3::6HA;4-Myc::rab11a* (*DTS1*) and *DTS1;Δdhc3* parasites. Parasites were co-stained with antibodies against Myc and PolyE. PolyE is a marker for the stabilized MT. Scale bars: 5 μm. Three independent experiments. **B** U-ExM of SPMTs and Rab11B in early ookinetes of the *dhc3::6HA;4Myc::rab11b* (*DTS2*) and *DTS2;Δdhc3* parasites. Parasites were co-stained with antibodies against Myc and PolyE. Scale bars: 5 μm. Three independent experiments. **C** U-ExM of SPMTs and DHC3 in early ookinetes of the

dhc3::6HA, dhc3::6HA;rab11a-DN, and dhc3::6HA;rab11a-CA parasites. Parasites were co-stained with antibodies against PolyE and HA. Scale bars: 5 μm. Three independent experiments. **D** U-ExM of SPMTs and DHC3 in early ookinetes of the dhc3::6HA, dhc3::6HA;rab11b-DN, and dhc3::6HA;rab11b-CA parasites. Parasites were co-stained with antibodies against PolyE and HA. Scale bars: 5 μm. Three independent experiments. **E** A schematic showing the position relationship of SPMT-based motor machinery composing the dynein, Rab receptors (Rab11A and Rab11B), and cargo (not shown) in ookinetes.

transport driven by a set of myosin motors and Rab proteins is likely responsible for protein trafficking from the Golgi to the apical end  $^{55}$ . For sporozoites, it is unclear which mode is used and DHC3 involvement in sporogony could be tested by stage-specific deletion of the gene. Also, the number (approximately 60) of SPMTs in the ookinetes is much higher than that (approximately 1–9) in merozoites  $^{8,12}$  and the SPMTs in ookinetes are 10– $15\,\mu m$  in length compared to 0.5– $1\,\mu m$  in merozoites  $^{9,11}$ . Compared to erythrocytic schizogony, ookinete growth likely requires much more long-distance cargo transport from the cell body to the apical distal for material trafficking. Although the SPMT

cytoskeletons are analogously essential in all three zoite stages, the requirement of SPMT-based cytoplasmic dynein and dynein-driven cargo transport may be zoite stage-specific.

Kinesins are MT-based molecular motors that dominantly move toward the plus end of MT<sup>24</sup>. Approximately 9 putative kinesins are encoded in the *Plasmodium* genome<sup>56</sup>. The developmental stage expression and subcellular localization of all 9 kinesins were recently investigated in *P. berghet*<sup>57</sup>. Among the kinesins analyzed, Kinesin-X3 showed a peripheral distribution restricted to one side of the early ookinetes but enveloped the entire periphery in mature ookinetes<sup>57</sup>,



suggesting a possible SPMT association. Whether Kinesin-X3 is an SPMT-based motor and whether Kinesin-X3 plays a role in ookinete development are worth investigating in the future.

The DHC3-deficient parasites showed severely defective development in the ookinete apical part, especially the formation of SPMTs, APR, and ATR. In addition, they were impaired in the distribution and

secretion of micronemes. To fit the requirement of material transport, many different vesicle cargoes should be loaded into the SPMT-based dynein and delivered toward the apical direction. This raises the question of how the dynein motor recognizes the cargo vesicles for transport. Rab protein has been reported as the receptor for the cargo in eukaryotic intracellular vesicle trafficking<sup>58</sup>. In this study, we

Fig. 10 | Disturbing Rab11A or Rab11B phenocopies DHC3 deficiency in ookinete morphogenesis. A Parasite asexual blood stage proliferation in mice for the 17XNL, rab11a-CA, and rab11a-DN. Values are means  $\pm$  SEM (n = 3 biological replicates). **B** Gametocyte formation in mice. Values are means  $\pm$  SEM (n = 3 biological replicates). **C** Ookinete formation in vitro. Values are means  $\pm$  SEM (n = 3 biological replicates). Two-sided t-test. **D** Ookinete formation in the mosquito midgut. Values are means  $\pm$  SEM (n = 3 biological replicates). Two-sided t-test. **E** IFA of P28 in ookinete and early oocyst at mosquito midguts infected with 17XNL and rab11a-DN 24 hpi. Scale bars: 10 μm. The right panel shows the quantification of parasites per midgut. x/y on the top is the count of midguts containing parasites/the count of midguts measured. Red horizontal lines show the mean value. Two-sided Mann–Whitney *U*-test. Three independent experiments. **F** Midgut oocyst formation in mosquito 7 dpi. n is the number of mosquitoes dissected. Red horizontal lines show the mean value. Two-sided Mann-Whitney U-test. Three independent experiments. G Salivary gland sporozoite counts in mosquitoes 14 dpi. 30 mosquitoes were dissected in each group per replicate. Values are means  $\pm$  SEM (n = 3 biological replicates). Two-sided t-test. **H** Parasite asexual blood stage proliferation in mice for the 17XNL, rab11b-CA, and rab11b-DN in mice. Values are means ± SEM (n=3 biological replicates). I Gametocyte formation in mice. Values are means  $\pm$ SEM (n = 3 biological replicates). I Ookinete formation in vitro. Values are means  $\pm$  SEM (n = 3 biological replicates). Two-sided t-test. **K** Ookinete formation in the mosquito midgut. Values are means  $\pm$  SEM (n = 3 biological replicates). Twosided t-test. L IFA of P28 in ookinete and early oocyst at mosquito midguts infected with 17XNL and rab11b-DN 24 hpi. Scale bars: 10 µm. The right panel shows the quantification of parasites per midgut. x/y on the top is the count of midguts containing parasites/the count of midguts measured. Red horizontal lines show the mean value. Two-sided Mann-Whitney U-test. Two independent experiments. **M** Midgut oocyst formation in mosquitoes 7 dpi. *n* is the number of mosquitoes dissected. Two-sided Mann-Whitney *U*-test. Three independent experiments. N Salivary gland sporozoite counts in mosquitoes 14 dpi. 30 mosquitoes were dissected in each group per replicate. Values are means  $\pm$  SEM (n=3 biological replicates). Two-sided t-test. Source data are provided as a Source Data file.

characterized Rab11A and Rab11B both of which are associated with DHC3 and co-localizing with SPMTs in the ookinetes. Functional disturbing of either single Rab11A or Rab11B via DN inhibition resulted in ookinete development arrest that mimicked the defects caused by DHC3 disruption. Another study also revealed that Rab11A is localized at the periphery of the ookinetes and is essential for the ookinete development of P. berghei<sup>45</sup>. Consistent with the cargo receptor role, Rab11A and Rab11B require dynein for their SPMT association. The Rab11A- and Rab11B-vesicles may be dominant cargo vesicles driven by the SPMT-based dynein. Although dynein can transport different vesicle cargoes, establishing a functional dynein-cargo link depends on a cargo-specific activating adapter as the dynein complex has not been reported to interact directly with the Rab proteins<sup>25,59</sup>. In eukaryotes, the Rab11-interacting proteins (FIPs) play an adapter role for the dynein complex linking with the Rab11A-vesicles<sup>60</sup>. However, no homologs of different FIP proteins could be found in the *Plasmodium* genome. Another future avenue of investigation is elucidating the adapter protein linking dynein with the Rab11A- and Rab11B-vesicles in the ookinetes. Based on the results of this and other studies, we proposed a working model (Fig. S9) that the SPMT-based dynein motor function to deliver the Rab11A- and Rab11B-vesicles likely containing materials to the apical for apical organelles assembly in the ookinetes.

# **Methods**

## **Ethics statement**

The animal experiments conducted in this study were approved by the Committee for Care and Use of Laboratory Animals of Xiamen University (XMULAC20190001).

#### Mice and mosquito usage

Female ICR mice (5–6 weeks old) were obtained from the Animal Care Center of Xiamen University and used for parasite propagation, drug selection, parasite cloning, and mosquito feeding. The larvae of *Anopheles stephensi* mosquitoes (*Hor* strain) were reared at 28 °C, 80% relative humidity, and a 12-h light/12-h dark condition in a standard insect facility. Adult mosquitoes were supplemented with 10% (w/v) sugar solution containing 0.05% 4-aminobenzoic acid and kept at 23 °C.

## Plasmid construction and parasite transfection

The CRISPR-Cas9 plasmid pYCm was used for gene editing<sup>30</sup>. To construct vectors for gene deletion, the left and right homologous arms consisted of 400–700 bp sequences upstream and downstream of the coding sequences of the target gene. To construct plasmids for gene tagging, the 5′- and 3′-flanking sequences (300–700 bp) at the designed insertion site of target genes were amplified as homologous templates. DNA fragments encoding 6HA,

4Myc, 3V5, and mScarlet were placed between them and in-frame with the target gene. For each modification, at least two small guide RNAs (sgRNAs) were designed using the online program EuPaGDT (http://grna.ctegd.uga.edu/). To construct the plasmids for overexpression of the rab genes, the expression cassettes of rab genes driven by the 5'-UTR (1755 bp) of the hsp70 gene and the 3'-UTR (561 bp) of the dhfr gene were inserted into specific restriction sites between the left and right homologous arms for transgenic integration in the p230p locus of P. yoelit<sup>61</sup>. Paired oligonucleotides for sgRNA were denatured at 95 °C for 3 min, annealed at room temperature for 5 min, and ligated into pYCm. All primers and oligonucleotides used in the plasmid construction are listed in Supplementary Table 1. For parasite electroporation, parasiteinfected red blood cells were electroporated with 5 µg plasmid DNA using Lonza Nucleofector. Transfected parasites were immediately intravenously injected into a naïve mouse and exposed to pyrimethamine (6 mg/ml) provided in mouse drinking water 24 h after transfection.

#### Genotyping of genetically modified parasites

All modified or transgenic parasites were generated from the P. yoelii 17XNL strain or 17XNL-derived lines (Supplementary Table 2).  $10\,\mu l$ parasite-infected blood was collected from the infected mice tail vein and red blood cells were lysed using 1% saponin in PBS. Parasite cells were spun down by centrifugation at  $13,000 \times g$  for 5 min and pellets were washed twice with PBS and boiled at 95 °C for 10 min followed by centrifugation at  $13,000 \times g$  for 5 min. The supernatant containing parasite genomic DNA was subjected to genotyping. For each gene modification, both the 5' and 3' homologous recombination events were detected by diagnostic PCR, confirming the successful integration of the homologous templates. Parasite clones with targeted modifications were obtained by limiting dilution cloning. At least two clones of each gene-modified parasite were used for phenotypic analysis. Modified parasite clones subject to additional modification were negatively selected to remove pYCm plasmid. Each naïve mouse infected with the pYCm plasmid-carrying parasites was exposed to 5-Fluorouracil (5-FC, Sigma-Aldrich, cat#F6627) in mouse drinking water (2.0 mg/ml). After 3 days, most of the surviving parasites no longer carried pYCm plasmids and underwent limiting dilution cloning by injecting them into mice via the tail vein. Seven days later, blood smears were used to identify the mice that were infected with parasites, and these parasites were genotyped again and used as a single clone.

#### Parasite intraerythrocytic asexual proliferation in mouse

Parasite proliferation rates in the asexual blood stage were determined in mice. Four ICR mice were included in each group. Parasite growth was monitored by Giemsa-stained thin blood smears every two days from day 2 to 14 after intravenous injection of  $1.0 \times 10^5$  parasites. The parasitemia was calculated as the ratio of parasitized erythrocytes over total erythrocytes.

#### Gametocyte induction in mouse

ICR mice were treated with phenylhydrazine (80  $\mu$ g/g mouse body weight; Sangon Biotech, China, cat#A600705-0025) through intraperitoneal injection. Three days after treatment, the mice were infected with  $5.0 \times 10^6$  parasites via intravenous injection. The peak of gametocytaemia usually occurs on day three post-infection. Male and female gametocytes were checked via Giemsa-stained thin blood smears. Gametocytemia was calculated as a percentage of the number of male or female gametocytes over the number of parasitized erythrocytes.

#### **Exflagellation assay**

 $2.5\,\mu l$  of mouse tail blood containing gametocytes was mixed with  $100\,\mu l$  of exflagellation medium. The exflagellation medium was composed of RPMI 1640 supplemented with  $100\,\mu M$  xanthurenic acid (XA, Sigma-Aldrich, cat#D120804), 2 unit/ml heparin, and pH 7.4. The mixture was incubated at 22 °C for 10 min. The number of parasite exflagellation centers (ECs) and total red blood cells were counted within a  $1\times 1$ -mm square area of a hemocytometer under a light microscope. The exflagellation rate was calculated as the number of ECs per 100 male gametocytes. Three biological replicates were conducted for each exflagellation assay.

#### In vitro ookinete culture and purification

Mouse blood with 6-10% gametocytemia was collected and immediately mixed with ookinete culture medium (RPMI 1640, 10% FCS, 100 µM XA, 25 mM HEPES, 0.1 mg/ml streptomycin, 100 U/ml penicillin, pH 8.0). The gametocyte-containing mouse blood was cultured at 22 °C for 12-15 h for gametogenesis, fertilization, and ookinete differentiation. Ookinetes formation was evaluated based on cell morphology in Giemsa-stained thin blood smears. The mature ookinete conversion rate was calculated as the number of crescent-shaped mature ookinete (stage V) over that of total ookinetes (from stage I to V). Ookinetes were purified using Nycodenz density gradient centrifugation as described previously<sup>62</sup>. After centrifugation at 500 × g for 5 min, ookinete pellets were resuspended with 7 ml PBS and transferred onto the top of 2 ml of 63% Nycodenz (Axis-shield, cat#66108-95-0) in a 15 ml Falcon tube. After centrifuging at  $1000 \times g$ for 20 min, the ookinetes enriched at the interface layer were collected from the Falcon tube. The purity of ookinetes was examined by hemocytometer analysis. Ookinetes with more than 80% purity were used for further experiments.

#### Parasite infection and transmission in mosquito

Forty female *Anopheles stephensi* mosquitoes in one cage were allowed to feed on one anesthetized mouse carrying 6–10% gametocytemia for 30 min. For midgut oocyst counting, mosquito midguts were dissected on day 7 or 8 post-blood feeding and stained with 0.1% mercurochrome for oocyst observation. For salivary gland sporozoite counting, mosquito salivary glands were dissected on day 14 post blood feeding, and the average number of sporozoites per mosquito was calculated. For mice infected with sporozoite, 20 infected mosquitoes on day 14 post blood feeding were allowed to bite one anesthetized naïve mouse for 30 min. Parasite transmission capability from mosquito to mouse was monitored daily by Giemsa-stained blood smears for 12 days.

#### Ookinete microneme secretion assay

Microneme-secreted proteins were examined in the supernatant from the in vitro ookinete culture as previously reported<sup>63</sup>.  $5.0 \times 10^6$  purified

ookinetes were incubated in 200  $\mu$ l PBS at 22 °C to allow microneme protein secretion. After 6 h incubation, the supernatant was collected by centrifugation at 750 × g for 3 min, filtered through a 0.45  $\mu$ m filter (Millipore, cat#SLHP033RS). An equal volume of 2× Laemmli sample buffer was added. All samples were boiled at 95 °C for 10 min and centrifuged at 12,000 × g for 5 min. An equal volume of supernatant from each group was used for immunoblot analysis.

## Ookinete gliding assay

All procedures were performed in a temperature-controlled room at 22 °C. 20  $\mu$ l of the suspended ookinete cultures were mixed with 20  $\mu$ l of Matrigel (BD Biosciences, cat#356234) on ice. The ookinete and Matrigel mixtures were transferred onto a slide, covered with a coverslip, and sealed with nail varnish. The slide was rested for 30 min before observation under the microscope. After tracking a gliding ookinete under the microscope, time-lapse videos (1 frame per 20 s, for 20 min) were taken to track ookinete movement using a Nikon ECLIPSE E100 microscope fitted with an ISH500 digital camera controlled by ISCapture v3.6.9.3N software (Tucsen). Ookinete motility speeds were calculated with ImageJ software using the MtrackJ plugin  $^{64}$ .

#### DNA content measurement in ookinete

To evaluate nuclear DNA content changes from zygote to ookinete development post-fertilization, parasites were fixed using 4% paraformaldehyde for 20 min at 0 and 4 h from the ookinete culture medium, rinsed twice with PBS, and blocked with 5% BSA solution in PBS for 1 h. Parasites were then incubated with anti-P28 antibody for 1 h and washed with PBS three times. After this, parasites were incubated with fluorescent conjugated secondary antibodies for 1 h and followed by three washes with PBS. Parasites were then stained with DNA dye Hoechst 33342 (Thermo Fisher Scientific, cat#23491-52-3) for 10 min and mounted in a 90% glycerol solution. Female gametocytes (P28-negative), female gametes(P28-positive), and zygotes (P28-positive) were measured for the Hoechst 33342 signal. Images were captured using identical settings under a ZEISS LSM 880 confocal microscope.

#### Antibodies and antiserum

The primary antibodies used included: rabbit anti-HA (Cell Signaling Technology/CST, cat#3724S, 1:1000 for immunoblotting (IB), 1:500 for immunofluorescence (IF), 1:500 for immunoprecipitation (IP)), mouse anti-HA(CST, cat#2367S, 1:500 for IF), rabbit anti-Myc (CST, cat#2272S, 1:1000 for IB, 1:500 for IF), mouse anti-Myc (CST, cat#2276S, 1:500 for IF, 1:1000 for IB, 1:500 for IP), mouse anti-α-tubulin II (Sigma-Aldrich, cat#T6199, 1:1000 for IF, 1:1000 for IB), mouse anti-β-tubulin (Sigma-Aldrich, cat#T5201, 1:1000 for IF, 1:1000 for IB), and rabbit anti-Polyglutamate chain (PolyE, AdipoGen, cat#AG-25B-0030, 1:1000 for IF). The secondary antibodies included: HRP-conjugated goat antirabbit IgG (Abcam, cat#ab6721, 1:5000 for IB), HRP-conjugated goat anti-mouse IgG (Abcam, cat#ab6789, 1:5000 for IB), Alexa 555 goat anti-rabbit IgG (Thermo Fisher Scientific, cat#A21428, 1:1000 for IF), and Alexa 488 goat anti-mouse IgG (Thermo Fisher Scientific, cat#A11001, 1:1000 for IF). The anti-serums, including the rabbit anti-P28 (1:1000 for IB, 1:1000 for IF), rabbit anti-BiP (1:1000 for IB), rabbit anti-Enolase (1:1000 for IB), rabbit anti-Rab11A (1:500 for IB), rabbit anti-GAP45 (1:1000 for IF), rabbit anti-WARP (1:1000 for IB), rabbit anti-CTRP (1:1000 for IB, 1:1000 for IF) and rabbit anti-chitinase (1:1000 for IB, 1:1000 for IF).

## Immunofluorescence assay

Parasites fixed in 4% paraformaldehyde were transferred to a Poly-L-Lysine coated coverslip in a 24-well plate and centrifuged at  $550 \times g$  for 5 min. Parasites were then permeabilized with 0.1% Triton X-100 solution in PBS for 10 min, blocked in 5% BSA solution in PBS for 60 min at room temperature, and incubated with the primary

antibodies diluted in 5% BSA-PBS for 1 h at room temperature. After three PBS washes, the coverslip was incubated with fluorescent conjugated secondary antibodies for 1 h at room temperature. Cells were stained with Hoechst 33342, mounted in 90% glycerol solution, and sealed with nail varnish. All images were acquired and processed using identical settings on Zeiss LSM 880 or LSM 980 confocal microscopes.

#### Live cell imaging

Parasites expressing the mScarlet-fused proteins were collected in 200  $\mu$ l PBS, washed three times with PBS, and stained with Hoechst 33342 at room temperature for 10 min. After centrifugation at  $500\times g$  for 3 min, the parasite pellets were resuspended in  $100\,\mu$ l of 3% low melting agarose (Sigma-Aldrich, A9414), and transferred evenly on the bottom of a 35-mm culture dish. Parasites were placed at room temperature for 15 min and imaged using a Zeiss LSM 880 confocal microscope.

#### Fluorescence recovery after photobleaching (FRAP) assay

A laser pulse was used to bleach 80–90% of the mScarlet fluorescence at a rectangle region in the ookinete periphery of the parasite *dhc3::mScarlet*. Another ookinete in the same field was set as a no-photobleaching control. The recovery of fluorescence in the rectangle region was monitored. Images were taken in a time-series mode to record the fluorescent signal intensities using a Zeiss LSM 980 confocal microscope. The time-series parameters for acquiring images were set as follows: scanning every 1 s for 30 s. Twenty ookinetes were analyzed in each group.

#### Protein extraction and immunoblot

Parasites were lysed in RIPA buffer (0.1% SDS, 1 mM DTT, 50 mM NaCl, 20 mM Tris-HCl; pH 8.0) (Solaribio, cat#R0010) supplemented with protease inhibitor cocktail (Medchem Express, cat#HY-K0010) and PMSF (Roche, cat#10837091001). After ultrasonication, the extracts were incubated on ice for 30 min followed by centrifugation at 12,000 × g for 10 min at 4 °C. The clarified supernatant was mixed with the same volume of 2× Laemmli sample buffer, boiled at 95 °C for 5 min, and cooled at room temperature. After SDS-PAGE separation, samples were transferred to a PVDF membrane (Millipore, cat#IPVH00010). The membrane was blocked with 5% skim milk, probed with primary antibodies for 1 h at room temperature, rinsed 3 times with TBST, and incubated with HRP-conjugated secondary antibodies. Followed by three washes with TBST, the membrane was visualized with enhanced chemiluminescence detection (Advansta, cat#K12045-D10).

#### **Protein immunoprecipitation**

Parasites were lysed in the IP buffer A (50 mM HEPES pH 7.5, 150 mM NaCl, 1 mM EDTA, 1 mM EGTA, 1% Triton X-100, 0.1% sodium deoxycholate) with protease inhibitor cocktail and PMSF. Protein aggregates were pre-cleared by centrifugation at  $20,000\times g$  for 10 min, and 1 ml of lysates were incubated with primary beads (anti-HA or anti-Myc nanobody) mixed for 3 h. The beads were washed with IP buffer A three times at 4 °C, and then mixed with an equal volume of  $2\times 10^{-10}$  Laemmli sample buffer for protein elution. All samples were boiled at  $2\times 10^{-10}$  min and centrifuged at  $2\times 10^{-10}$  min. An equal volume of supernatant from each sample was used for immunoblotting.

## Extraction of ookinete pellicle cytoskeleton

Extraction of ookinete pellicle cytoskeleton was performed as previously described <sup>38</sup>. Approximately  $5.0 \times 10^6$  purified ookinetes were lysed in 200  $\mu$ l 0.5 mM sodium deoxycholate (SDC) detergent for 3 min at room temperature. Followed by centrifugation at  $800 \times g$  for 8 min, the pellet fractions containing ookinete cytoskeleton were collected for further experiments.

#### Scanning electron microscopy

Purified ookinetes were fixed with 2.5% glutaraldehyde in 0.1 M phosphate buffer at 4 °C overnight, rinsed three times with PBS, and fixed with 1% osmium tetroxide for 2 h. Fixed cells were dehydrated using a graded acetone series,  $CO_2$ -dried in a critical-point drying device, and gold-coated in a sputter coater as detailed previously<sup>65</sup>. The samples were imaged using a SUPRA55 SAPPHIRE Field Emission Scanning Electron Microscope.

#### **Transmission electron microscopy**

Purified ookinetes were fixed with 2.5% glutaraldehyde in 0.1 M phosphate buffer at 4 °C overnight, as previously described<sup>4</sup>. Samples were post-fixed in 1% osmium tetroxide at 4 °C for 2 h, treated *en bloc* with uranyl acetate, dehydrated, and embedded in Spurr's resin. Thin sections were sliced, stained with uranyl acetate and lead citrate, and examined in an HT-7800 electron microscope (Hitachi, Japan).

#### Ultrastructure expansion microscopy (U-ExM)

Purified ookinetes were sedimented on a 15 mm round poly-D-lysine (Sigma-Aldrich, cat#A-003-M) coated coverslips for 10 min. The parasites were then permeabilized with 100% ice-cold methanol for 7 min. To add anchors to proteins, coverslips were incubated for 5 h in 1.4% formaldehyde (FA, Sigma-Aldrich, cat#F8775)/2% acrylamide (AA, Sigma-Aldrich, cat#146072) at 37 °C. Next, gelation was performed in ammonium persulfate (APS, Sigma-Aldrich, cat#A7460)/ N,N,N',N '-Tetramethyl ethylenediamine (Temed, Sigma-Aldrich, cat#110-18-9)/ Monomer solution (23% Sodium Acrylate (SA, Sigma-Aldrich, cat#408220); 10% AA; 0.1% N,N'-Methylenebisacrylamide (BIS-AA, Sigma-Aldrich, cat#M7279) in PBS) for 1h at 37 °C. Sample denaturation was performed for 90 min at 95 °C. Gels were incubated in bulk ddH<sub>2</sub>O at room temperature overnight for complete expansion. In the following day, gel samples were washed in PBS twice for 30 min each to remove excess ddH<sub>2</sub>O. Gels were then cut into square pieces (1 cm × 1 cm), incubated with primary antibodies at 37 °C for 3 h, and washed with 0.1% PBS-Tween (PBS-T) 3 times for 10 min each. Incubation with the secondary antibodies was performed for 3 h at 37 °C followed by three washes with 0.1% PBS-T for 10 min each. In some conditions, gels were additionally stained by NHS-ester (Merck, cat#08741) diluted at 10 µg/ml in PBS for 90 min at room temperature. After the final staining step, gels were then washed with 0.1% PBS-T three times for 15 min each and expanded overnight by incubating in bulk ddH<sub>2</sub>O at room temperature. After the second round of expansion, gels were cut into square pieces (0.5 cm × 0.5 cm) and mounted by a coverslip in a fixed position for imaging.

## **Proximity ligation assay (PLA)**

PLA assay was performed to detect in situ protein interaction using a commercial kit (Sigma-Aldrich, cat#DUO92008, DUO92001, DUO92005, and DUO82049). Ookinetes were fixed with 4% paraformaldehyde for 30 min, permeabilized with 0.1% Triton X-100 for 10 min at room temperature, and blocked with a blocking solution overnight at 4 °C. The primary antibodies were diluted in the Duolink Antibody Diluent and incubated with ookinetes in a humidity chamber overnight at 4 °C. After removing the primary antibodies, the ookinetes were rinsed twice with wash buffer A. The PLUS and MINUS PLA probes were diluted in Duolink Antibody Diluent and ookinetes were incubated in a humidity chamber for 1 h at 37 °C. Next, ookinetes were rinsed twice with wash buffer A and incubated with the ligation solution for 30 min at 37 °C. Followed by twice rinses with wash buffer A, ookinetes were incubated with the amplification solution for 100 min at 37 °C in the dark. After rinsing twice with 1× wash buffer B and once with 0.01× wash buffer B, ookinetes were stained with Hoechst 33342 and washed twice with PBS. Images were captured and processed using identical settings on a Zeiss LSM 880 confocal microscope.

#### Software, program, database, and tool used

The genomic sequences of parasite genes are downloaded from the PlasmoDB database (https://plasmodb.org/plasmo/app/)66. We provided a table (Supplementary Table 3) showing all homologs for the seven putative DHC proteins in three *Plasmodium* species including *P*. voelii, P. berghei, and P. falciparum. The sgRNA of target genes are designed using the program EuPaGDT (http://grna.ctegd.uga.edu/)<sup>67</sup>. For quantification of protein expression in immunoblot, the blot band intensity is quantified using Fiji software<sup>68</sup>. For quantification of protein expression in IFA, images are acquired under identical parameters. Fluorescent signals are quantified using ZEN Microscopy Software from ZEISS, and 20 cells are chosen in each group. The 3D surface topology reconstruction of Z-stack images is quantified by Imaris X64 9.2.0. All graph-making and statistical analysis was performed using GraphPad Prism 8.0 with either a two-tailed Student's t-test or Mann–Whitney *U*-test as appropriate. Data collected as raw values are shown as mean ± SEM or mean ± SD or means only if not otherwise stated. Details of statistical methods are reported in the figure legends. p-values were indicated in the figures with a value < 0.05 considered significant. n represents the sample size in each group or the number of biological replicates.

#### Reporting summary

Further information on research design is available in the Nature Portfolio Reporting Summary linked to this article.

## Data availability

All relevant data in this study are submitted as supplementary source files. Source data are provided with this paper.

#### References

- World Health Organization. World Malaria Report 2020 (World Health Organization, Geneva, Switzerland, 2020).
- Bennink, S., Kiesow, M. J. & Pradel, G. The development of malaria parasites in the mosquito midgut. *Cell Microbiol.* 18, 905–918 (2016).
- Guttery, D. S., Roques, M., Holder, A. A. & Tewari, R. Commit and transmit: molecular players in plasmodium sexual development and zygote differentiation. *Trends Parasitol.* 31, 676–685 (2015).
- Wang, X., Qian, P., Cui, H., Yao, L. & Yuan, J. A protein palmitoylation cascade regulates microtubule cytoskeleton integrity in Plasmodium. EMBO J. 39, e104168 (2020).
- Aly, A. S., Vaughan, A. M. & Kappe, S. H. Malaria parasite development in the mosquito and infection of the mammalian host. *Annu. Rev. Microbiol.* 63, 195–221 (2009).
- Kono, M., Prusty, D., Parkinson, J. & Gilberger, T. W. The apicomplexan inner membrane complex. Front. Biosci. 18, 982–992 (2013).
- Morrissette, N. S. & Sibley, L. D. Cytoskeleton of apicomplexan parasites. *Microbiol. Mol. Biol. Rev.* 66, 21–38 (2002).
- Bertiaux, E. et al. Expansion microscopy provides new insights into the cytoskeleton of malaria parasites including the conservation of a conoid. PLoS Biol. 19, e3001020 (2021).
- Spreng, B. et al. Microtubule number and length determine cellular shape and function in Plasmodium. EMBO J. 38, e100984 (2019).
- Harding, C. R. & Frischknecht, F. The riveting cellular structures of apicomplexan parasites. *Trends Parasitol.* 36, 979–991 (2020).
- 11. Ferreira, J. L. et al. Variable microtubule architecture in the malaria parasite. *Nat. Commun.* **14**, 1216 (2023).
- Fowler, R. E., Fookes, R. E., Lavin, F., Bannister, L. H. & Mitchell, G. H. Microtubules in Plasmodium falciparum merozoites and their importance for invasion of erythrocytes. *Parasitology* 117, 425–433 (1998).

- Qian, P. et al. Apical anchorage and stabilization of subpellicular microtubules by apical polar ring ensures Plasmodium ookinete infection in mosquito. Nat. Commun. 13, 7465 (2022).
- Raibaud, A. et al. Cryofracture electron microscopy of the ookinete pellicle of Plasmodium gallinaceum reveals the existence of novel pores in the alveolar membranes. J. Struct. Biol. 135, 47–57 (2001).
- Canning, E. U. & Sinden, R. E. The organization of the ookinete and observations on nuclear division in oocysts of Plasmodium berghei. *Parasitology* 67, 29–40 (1973).
- Cyrklaff, M. et al. Cryoelectron tomography reveals periodic material at the inner side of subpellicular microtubules in apicomplexan parasites. J. Exp. Med. 204, 1281–1287 (2007).
- Frenal, K. & Soldati-Favre, D. Role of the parasite and host cytoskeleton in apicomplexa parasitism. *Cell Host Microbe* 5, 602–611 (2009).
- Francia, M. E. & Striepen, B. Cell division in apicomplexan parasites. Nat. Rev. Microbiol. 12, 125–136 (2014).
- Sibley, L. D. Intracellular parasite invasion strategies. Science 304, 248–253 (2004).
- 20. Blackman, M. J. & Bannister, L. H. Apical organelles of Apicomplexa: biology and isolation by subcellular fractionation. *Mol. Biochem. Parasitol.* **117**, 11–25 (2001).
- Sweeney, H. L. & Holzbaur, E. L. F. Motor proteins. Cold Spring Harb. Perspect. Biol. https://doi.org/10.1101/cshperspect.a021931 (2018).
- 22. Downing, K. H. & Nogales, E. Tubulin and microtubule structure. *Curr. Opin. Cell Biol.* **10**, 16–22 (1998).
- 23. Nogales, E., Whittaker, M., Milligan, R. A. & Downing, K. H. Highresolution model of the microtubule. *Cell* **96**, 79–88 (1999).
- Hirokawa, N., Noda, Y., Tanaka, Y. & Niwa, S. Kinesin superfamily motor proteins and intracellular transport. *Nat. Rev. Mol. Cell Biol.* 10, 682–696 (2009).
- Reck-Peterson, S. L., Redwine, W. B., Vale, R. D. & Carter, A. P. The cytoplasmic dynein transport machinery and its many cargoes. *Nat. Rev. Mol. Cell Biol.* 19, 382–398 (2018).
- Schroer, T. A., Steuer, E. R. & Sheetz, M. P. Cytoplasmic dynein is a minus end-directed motor for membranous organelles. *Cell* 56, 937–946 (1989).
- 27. Viswanadha, R., Sale, W. S. & Porter, M. E. Ciliary motility: regulation of axonemal dynein motors. *Cold Spring Harb. Perspect. Biol.* **9**, a018325 (2017).
- Hook, P. & Vallee, R. B. The dynein family at a glance. J. Cell Sci. 119, 4369–4371 (2006).
- Zhang, C. et al. CRISPR/Cas9 mediated sequential editing of genes critical for ookinete motility in Plasmodium yoelii. *Mol. Biochem.* Parasitol. 212, 1–8 (2017).
- 30. Zhang, C. et al. Efficient editing of malaria parasite genome using the CRISPR/Cas9 system. *mBio* **5**, e01414-14 (2014).
- 31. Yusuf, N. A. et al. The plasmodium class XIV myosin, MyoB, has a distinct subcellular location in invasive and motile stages of the malaria parasite and an unusual light chain. *J. Biol. Chem.* **290**, 12147–12164 (2015).
- 32. Wall, R. J. et al. SAS6-like protein in Plasmodium indicates that conoid-associated apical complex proteins persist in invasive stages within the mosquito vector. Sci. Rep. 6, 28604 (2016).
- Gao, H. et al. ISP1-anchored polarization of GCbeta/CDC50A complex initiates malaria ookinete gliding motility. *Curr. Biol.* 28, 2763–2776.e6 (2018).
- Dessens, J. T. et al. CTRP is essential for mosquito infection by malaria ookinetes. EMBO J. 18, 6221–6227 (1999).
- Tsai, Y. L., Hayward, R. E., Langer, R. C., Fidock, D. A. & Vinetz, J. M. Disruption of Plasmodium falciparum chitinase markedly impairs parasite invasion of mosquito midgut. *Infect. Immun.* 69, 4048–4054 (2001).

- Dessens, J. T. et al. Knockout of the rodent malaria parasite chitinase pbCHT1 reduces infectivity to mosquitoes. *Infect. Immun.* 69, 4041–4047 (2001).
- 37. Alam, M. S. Proximity ligation assay (PLA). *Curr. Protoc. Immunol.* **123**, e58–e58 (2018).
- Wang, X. et al. Cryo-EM structure of cortical microtubules from human parasite Toxoplasma gondii identifies their microtubule inner proteins. Nat. Commun. 12, 3065 (2021).
- Long, S., Anthony, B., Drewry, L. L. & Sibley, L. D. A conserved ankyrin repeat-containing protein regulates conoid stability, motility and cell invasion in Toxoplasma gondii. *Nat. Commun.* 8, 2236 (2017).
- Gee, M. A., Heuser, J. E. & Vallee, R. B. An extended microtubulebinding structure within the dynein motor domain. *Nature* 390, 636–639 (1997).
- Carter, A. P. et al. Structure and functional role of dynein's microtubule-binding domain. Science 322, 1691–1695 (2008).
- Pfister, K. K. et al. Genetic analysis of the cytoplasmic dynein subunit families. PLoS Genet. 2, e1 (2006).
- 43. Stenmark, H. Rab GTPases as coordinators of vesicle traffic. *Nat. Rev. Mol. Cell Biol.* **10**, 513–525 (2009).
- 44. Bhuin, T. & Roy, J. K. Rab proteins: the key regulators of intracellular vesicle transport. *Exp. Cell Res.* **328**, 1–19 (2014).
- Patil, H. et al. Zygote morphogenesis but not the establishment of cell polarity in Plasmodium berghei is controlled by the small GTPase, RAB11A. PLoS Pathog. 16, e1008091 (2020).
- Otto, T. D. et al. A comprehensive evaluation of rodent malaria parasite genomes and gene expression. BMC Biol. 12, 86 (2014).
- Reddy, J. M., Raut, N. G. R., Seifert, J. L. & Hynds, D. L. Regulation of small GTPase prenylation in the nervous system. *Mol. Neurobiol.* 57, 2220–2231 (2020).
- Khandelwal, P. et al. Rab11a-dependent exocytosis of discoidal/ fusiform vesicles in bladder umbrella cells. *Proc. Natl Acad. Sci.* USA 105, 15773–15778 (2008).
- 49. Stone, R., Hayashi, T., Bajimaya, S., Hodges, E. & Takimoto, T. Critical role of Rab11a-mediated recycling endosomes in the assembly of type I parainfluenza viruses. *Virology* **487**, 11–18 (2016).
- Agop-Nersesian, C. et al. Rab11A-controlled assembly of the inner membrane complex is required for completion of apicomplexan cytokinesis. *PLoS Pathog.* 5, e1000270 (2009).
- 51. Venugopal, K. et al. Rab11A regulates dense granule transport and secretion during Toxoplasma gondii invasion of host cells and parasite replication. *PLoS Pathog.* **16**, e1008106 (2020).
- Allan, V. J. Cytoplasmic dynein. *Biochem. Soc. Trans.* 39, 1169–1178 (2011).
- 53. Ferreira, J. L. et al. The dynamic roles of the inner membrane complex in the multiple stages of the malaria parasite. *Front. Cell Infect. Microbiol.* **10**, 611801 (2020).
- Arnot, D. E., Ronander, E. & Bengtsson, D. C. The progression of the intra-erythrocytic cell cycle of Plasmodium falciparum and the role of the centriolar plaques in asynchronous mitotic division during schizogony. *Int. J. Parasitol.* 41, 71–80 (2011).
- 55. Mayer, D. C. G. Protein dorting in Plasmodium falciparum. *Life* https://doi.org/10.3390/life11090937 (2021).
- Zeeshan, M. et al. Plasmodium kinesin-8X associates with mitotic spindles and is essential for oocyst development during parasite proliferation and transmission. *PLoS Pathog.* 15, e1008048 (2019).
- Zeeshan, M. et al. Genome-wide functional analysis reveals key roles for kinesins in the mammalian and mosquito stages of the malaria parasite life cycle. *PLoS Biol.* 20, e3001704 (2022).
- Kjos, I., Vestre, K., Guadagno, N. A., Borg Distefano, M. & Progida, C. Rab and Arf proteins at the crossroad between membrane transport and cytoskeleton dynamics. *Biochim. Biophys. Acta Mol. Cell Res.* 1865, 1397–1409 (2018).

- McKenney, R. J., Huynh, W., Tanenbaum, M. E., Bhabha, G. & Vale, R.
   D. Activation of cytoplasmic dynein motility by dynactin-cargo adapter complexes. Science 345, 337–341 (2014).
- Wilson, G. M. et al. The FIP3-Rab11 protein complex regulates recycling endosome targeting to the cleavage furrow during late cytokinesis. *Mol. Biol. Cell* 16, 849–860 (2005).
- Liu, C. Y. et al. Generation of Plasmodium yoelii malaria parasite for conditional degradation of proteins. *Mol. Biochem. Parasitol.* https://doi.org/10.1016/j.molbiopara.2020.111346 (2021).
- Carter, V., Cable, H. C., Underhill, B. A., Williams, J. & Hurd, H. Isolation of Plasmodium berghei ookinetes in culture using Nycodenz density gradient columns and magnetic isolation. *Malar. J.* 2, 35 (2003).
- 63. Philip, N., Vaikkinen, H. J., Tetley, L. & Waters, A. P. A unique Kelch domain phosphatase in Plasmodium regulates ookinete morphology, motility and invasion. *PLoS ONE* **7**, e44617 (2012).
- 64. Meijering, E., Dzyubachyk, O. & Smal, I. Methods for cell and particle tracking. *Methods Enzymol.* **504**, 183–200 (2012).
- 65. Orfano, A. S. et al. Species-specific escape of Plasmodium sporozoites from oocysts of avian, rodent, and human malarial parasites. *Malar. J.* **15**, 394 (2016).
- 66. Aurrecoechea, C. et al. PlasmoDB: a functional genomic database for malaria parasites. *Nucleic Acids Res.* **37**, D539–D543 (2009).
- 67. Peng, D. & Tarleton, R. EuPaGDT: a web tool tailored to design CRISPR guide RNAs for eukaryotic pathogens. *Micro Genom.* **1**, e000033 (2015).
- 68. Schindelin, J. et al. Fiji: an open-source platform for biologicalimage analysis. *Nat. Methods* **9**, 676–682 (2012).

## **Acknowledgements**

This work was supported by the National Natural Science Foundation of China (32170427 to J.Y., 32270503 to H.C.), the Natural Science Foundation of Fujian Province (2021J01028 to J.Y.), the 111 Project sponsored by the State Bureau of Foreign Experts and Ministry of Education of China (BP2018017 to J.Y.), and the Xiamen University Double First Class Construction Project (Biology, DFC2024001 to J.Y.).

## **Author contributions**

B.L. and J.Y. designed the project. B.L., C.L., Z.L., and W.L., generated the modified parasites. B.L., C.L., and Z.L. performed phenotype analysis, protein analysis, imaging analysis, and electron microscopy analysis. B.L. performed the bioinformatics analysis. H.C. and J.Y. supervised the work. B.L., H.C., and J.Y. wrote the manuscript.

# **Competing interests**

The authors declare no competing interests.

## **Additional information**

**Supplementary information** The online version contains supplementary material available at https://doi.org/10.1038/s41467-024-52970-7.

**Correspondence** and requests for materials should be addressed to Huiting Cui or Jing Yuan.

**Peer review information** *Nature Communications* thanks Sabrina Absalon and the other, anonymous, reviewer(s) for their contribution to the peer review of this work. A peer review file is available.

**Reprints and permissions information** is available at http://www.nature.com/reprints

**Publisher's note** Springer Nature remains neutral with regard to jurisdictional claims in published maps and institutional affiliations.

Open Access This article is licensed under a Creative Commons Attribution-NonCommercial-NoDerivatives 4.0 International License, which permits any non-commercial use, sharing, distribution and reproduction in any medium or format, as long as you give appropriate credit to the original author(s) and the source, provide a link to the Creative Commons licence, and indicate if you modified the licensed material. You do not have permission under this licence to share adapted material derived from this article or parts of it. The images or other third party material in this article are included in the article's Creative Commons licence, unless indicated otherwise in a credit line to the material. If material is not included in the article's Creative Commons licence and your intended use is not permitted by statutory regulation or exceeds the permitted use, you will need to obtain permission directly from the copyright holder. To view a copy of this licence, visit <a href="https://creativecommons.org/licenses/by-nc-nd/4.0/">https://creativecommons.org/licenses/by-nc-nd/4.0/</a>.

© The Author(s) 2024